Green Synthesis of Silver Magnetite Nanocomposite Decorated Graphitic Carbon Nitride for Photocatalytic and Antibacterial Application

Redeat Solomon Garedew

A Thesis Submitted to the Department Applied Chemistry
School of Applied Natural Science

Presented in Partial Fulfillment of the Requirement for the Degree of Master Science in Applied Chemistry (Industrial Chemistry)

Office of Graduate Studies
Adama Science and Technology University

December, 2021
Adama, Ethiopia

Green Synthesis of Silver Magnetite Nanocomposite Decorated Graphitic Carbon Nitride for Photocatalytic and Antibacterial Application

Redeat Solomon Garedew

Major-advisor: Aschalew Tadesse (PhD)

Co-advisor: Bedasa Abdisa (PhD)

A Thesis Submitted to the Department of Applied Chemistry

School of Applied Natural Science

Presented in Partial Fulfillment of the Requirement for the Degree of Masters Science in Applied chemistry (Industrial Chemistry)

Office of Graduate Studies

Adama Science and Technology University

December, 2021

Adama, Ethiopia

Declaration

I hereby declare that this Master Thesis entitled "**Green Synthesis of Silver Magnetite Nanocomposite Decorated Graphitic Carbon Nitride for Photocatalytic and Antibacterial Application"** is my original work. That is, it has not been submitted for the award of any academic degree, diploma, or certificate in any other university. All sources of materials that are used for this thesis have been duly acknowledged through citation

_____	_____	_____
Name of the student	Signature	Date

Recommendation

We, the advisor of this thesis, hereby certify that we have read the revised version of the thesis entitled "**Green Synthesis of Silver Magnetite Nanocomposite Decorated Graphitic Carbon Nitride for Photocatalytic and Antibacterial Application"** prepared under our guidance by Redeat Solomon submitted in partial fulfillment of the requirements for the degree of Mater's of Science in Applied chemistry. Therefore, we recommend the submission of revised Version of the thesis to the department following the applicable procedures.

_____	_____	_____
Major-Advisor	Signature	Date
_____	_____	_____
Co-advisor	Signature	Date

Approval Sheet

We, the advisors of the thesis entitled "**Green Synthesis of Silver Magnetite Nanocomposite Decorated Graphitic Carbon Nitride for Photocatalytic and Antibacterial Application**" and developed by Redeat Solomon here certify that the recommendation and suggestions made by the broad of examiners are appropriately incorporated into the final version of the thesis.

_____	_____	_____
Major Advisor	Signature	Date
_____	_____	_____
Co-advisor	Signature	Date

We, the undersigned, members of the Board of Examiners of the thesis by Redeat Solomon have read and evaluated the thesis entitled "**Green Synthesis of Silver Magnetite Nanocomposite Decorated Graphitic Carbon Nitride For Photocatalytic and Antibacterial Application**" and examined the candidate during open defense. This is, therefore, to certify that the thesis is accepted for partial fulfillment of the requirement of the degree of Master of Science in Applied chemistry.

_____	_____	_____
Chairperson	Signature	Date
_____	_____	_____
Internal Examiner	Signature	Date
_____	_____	_____
External Examiner	Signature	Date

Final approval and acceptance of the thesis is contingent upon submission of its final copy To the Office of Postgraduate Studies (OPGS) through the Department Graduate Council (DGC) and School Graduate Committee (SGC).

_____	_____	_____
Department Head	Signature	Date
_____	_____	_____
School Dean	Signature	Date
_____	_____	_____
Office of Postgraduate Studies, Dean	Signature	Date

AKNOWLADGEMENT

First and foremost, I would like to thank the almighty God for his provisions and care throughout my academic journey. I would like to express my deepest thanks to my Advisor Dr. Aschalew Tadesse who has encouraged me to complete this research. I am thankful for his valuable advice and great support. Then I would like to express my genuine heartfelt gratitude to my co-advisor, Dr. Bedasa Abdisa

This study was impossible, thanks to my family. Without the support of them, especially my mother, I am deeply grateful for my family who has encouraged me not to give up.

I would like to express my sincere gratitude to all academic, technical, and support staff of the Program of Applied Chemistry, Adama Science and Technology University, providing the necessary knowledge, assistance, and facilities to conduct my research work.

Finally, I would like to thank my friends and classmates from whom we have learned much as a friend.

Table of Contents

List of Figure

List of Table

List of Abbreviations

AES	Auger Electron Spectra
ATP	Adenosine Triphosphate
BET	Brunauer–Emmett–Teller
CB	Conduction Band
DNA	Deoxyribonucleic Acid
E. coli	*Escherichia coli*
EDX	Energy Dispersive X-Ray Spectroscopy
EPMA	Electron Probe Microanalysis
EXAFS	Extended X-ray Absorption Fine Structure
FTIR	Fourier Transform Infrared
HNT	Halloysite Nanotubes
IONPS	Iron Oxide Nanoparticles
JCPDS	Joint Com-mittee on Powder Diffraction Standards
LEED	Low Energy Electron Diffraction
LSPR	localized Surface Plasma Resonance
MB	Methylene Blue
MNPs	Magnetite Nanoparticles
MtNPs	Metal Nanoparticles
NC	Nanocomposite
NPs	Nanoparticles
P. Aeruginosa	*Pseudomonas Aeruginosa*
RNA	Ribose Nucleic Acid

ROS	Reactive Oxygen Specious
S. Aureus	*Staphylococcus Aureus*
S. Pyogene	*Streptococcus Pyogenes*
SEM	Scanning Electron Microscopy
SIMS	Secondary Ion Mass Spectroscopy
SPR	Surface Plasmon Resonance
TEM	Transmission Electron Microscopy
UV-Vis	Ultraviolet Visible Spectroscopy
VB	Valance Band
XPS	X-Ray photoelectron spectroscopy
XRD	X-Ray Diffraction

Abstract

Nanotechnology is an advanced technology for environmental applications, including water treatment, detection of persistent pollutants, and antibacterial agent, are amongst many others. The reduction of dye compounds from industrial wastewater has been achieved using chemical, physical, and biological methods. However, these approaches are time-consuming, costly, and pose disposal problems. But complete mineralization with mild operating temperature and pressure can be achieved by Photocatalytic degradation by using a nanosized catalyst. The development of greenly synthesized Photocatalytic materials with antibacterial properties is highly desirable in wastewater treatment. In this study silver nanoparticles (Ag NPs), magnetite nanoparticles (Fe_3O_4 NPs), silver magnetite nanocomposite (Ag-Fe_3O_4 NC) were synthesized using an aqueous extract of Cymbopogon citratus leaves as a reducing agent and the synthesized Ag-Fe_3O_4 NC were decorated graphitic carbon nitride (g-C_3N_4) which was prepared by calcinations of urea. The synthesized nanomaterials were analyzed by Ultraviolet-Visible (UV-Vis) spectrophotometer, Fourier Transform Infrared (FTIR) spectrometer, X-Ray Diffraction (XRD), and Scanning Electron Microscope (SEM). In X-ray diffraction analysis of each synthesized materials show their representative peaks matched with their Joint Committee on Powder Diffraction Standards (JCPDS) card. The photocatalytic activities of Ag NPs, Ag-Fe_3O_4 NC and Ag-Fe_3O_4/g-C_3N_4 NC were evaluated by the degradation of methylene blue dye under visible light irradiation; the results indicated 86.31%, 89%, and 99.84% degradation efficiency of MB respectively by using pH10, 20 mg of catalyst, 20 ppm concentration of dye and 60 minute UV light irradiation. Furthermore, parameters such as the effect of pH of the dye solution, catalyst dose, dye concentration, and recyclability of Ag-Fe_3O_4/g-C_3N_4 NC was also studied. The antibacterial activity of synthesized nanomaterials was evaluated against Gram-negative and Gram-positive. Ag-Fe_3O_4/g-C_3N_4 NC demonstrated high-antibacterial activity, showed 20, 16mm for E. coli and P. Aeruginosa respectively, and 15 mm for S. Aureus and S. Pyogene.

***Keywords**:* Silver nanoparticles, magnetite nanoparticles, graphitic carbon nitride, Ag-Fe_3O_4/g-C_3N_4 nanocomposite and *Cymbopogon citratus*

CHAPTER ONE

1. Introduction

1.1. Background of Study

Nanotechnology is an emerging application in various fields such as medicine, biofuel production, wastewater engineering, drug delivery, etc. Nanoparticles are considered a fundamental unit of nanotechnology (Ijaz *et al*., 2020). Nanoparticles varied in size from 1 to 100 nm (Singh *et al*., 2020). Nanoparticles are used widely in environmental remediation for photodegradation, detection, selective removal, and adsorption of environmental pollutants (Guerra *et al*., 2018). Additionally, nanoparticles have been used as an antimicrobial agent; they are applied in textiles, home water purification systems, medical devices, cosmetics, electronics, and household appliances(Ijaz *et al*., 2020). Depending on the nature of the core materials, nanoparticles can have unique optical, electrical, and magnetic properties (Sajid *et al*., 2020).

There are more than 3000 azo dyes are widely used by the textile, leather, cosmetics, food coloring and paper production industries. About 80% of azo dyes are used in the dyeing process of textile industries. It had been estimated that approximately10% of the dyes used in dying process do not bind to the fiber and are released into the environment (Sandhya & Ramandeep, 2017). Among many synthetic dyes Congo red and methylene blue dyes were widely used in most of the industries. Methylene blue is a versatile compound which has wide range of applications. It is known to be an aromatic compound which is used in various fields. It has molecular formula $C_{16}H_{18}N_3SCl$ (Sandhya & Ramandeep, 2017). Methylene blue dyes is a model cationic dye employed by industries such as the textile industry for different purposes such as in coloring paper, dyeing cotton, wools, silk, leather, and coating for paper stock (Mulushewa *et al*., 2021). However, it has been posed environmental scientists' challenges due to their contradictory effects, such as minimizing light penetration can cause unpleasant damage to the aquatic environment, carcinogenesis, mutagenesis, and respiratory problem (Nguyen & Mousavi, 2020). Photocatalysis technology has been applied for environmental remediation owing to the advantage of transforming solar energy into chemical energy (Liu *et al*., 2020).

In photocatalytic processes, strong radicals are produced under light radiation, and these active species decompose organic pollutants into CO_2 and H_2O (Herrmann, 2005). The photocatalytic method benefits include its capability to consume renewable energy, mild reaction conditions, and an ability to reduce pollutants' toxicity and mineralize into low-harmful substances. Because of the reasons mentioned above, different studies have been done to modified and enhanced semiconductors to maximize their catalytic properties and to get excellent photocatalyst for the degradation of pollutants (Nguyen & Mousavi, 2020). In the photocatalytic degradation phenomenon, when a material is irradiated by UV light it generates electron-hole pair via undergoing a second order reaction kinetics with formation of free radical. These free radicals are considered as powerful oxidizing agents to degrade the toxic organic pollutants and micro pollutants present in the water (Khan *et al*., 2016). The nano-sized particles having large surface area due to their extremely smaller size are significant materials for photocatalysis (Mavaei *et al*., 2020). Among the various metal nanoparticles, silver nanoparticles, can demonstrate light absorption and significant visible light catalytic activity due to their narrow band gap energy to the many colorant/textile combinations under visible or sunlight illumination. Ag NPs possess good conductivity facilitating the transport of electrons (Khan *et al*., 2016). Many works have been devoted to improving charge separation in the semiconductor system. Combination of metallic or non-metallic elements to a semiconductor is one of the potential techniques to increase the photocatalytic efficiency of semiconductors (Joo *et al*., 2015; Kong *et al*., 2021; Yang *et al*., 2016).

More recently, graphitic carbon nitride (g-C_3N_4) has attracted increasing attention as a polymeric organic semiconductor visible-light-driven photocatalyst with a suitable band gap (Nguyen & Mousavi, 2020). Therefore, g-C_3N_4 become considered as an alternative candidate for solar light harvesting and conversion due to its many interesting features including visible-light absorption ability, environment-friendly characteristics, chemical stability, low cost, 2D structures, so forth (Zhang *et al.*, 2014). And also g-C_3N_4 used as metal-free disinfection were used to destroy pathogenic bacteria (Huang *et al*., 2014). Hence, the combination of graphitic carbon nitride with silver nanoparticle as the past studies (Liu *et al*., 2020) reported that the application of Ag/g-C_3N_4 in the degradation of organic pollutants is due to effect of SPR, the visible photocatalytic property and photoinduced electron−hole pair separation efficiency of

Ag/C_3N_4 were significantly higher than silver nanoparticles alone. Moreover heterogeneous photocatalysis is a promising strategy for advanced oxidation environmental remediation (Xin *et al*., 2020; Xin Li *et al*., 2020).

However, Ag/g-C_3N_4 suffers from different limitation, it can only absorb small fraction of the solar energy with wavelengths shorter than about 460nm and recombination of its photogenerated electron hole pairs are fast, leading to low photocatalytic activity and, it cannot be easily recycled from the treated solutions, resulting in generation of secondary pollution (Akhundi & Habibi, 2016). Therefore, to overcome these drawbacks the present study introduced magnetite (Fe_3O_4) nanoparticles to Ag/C_3N_4 composites because magnetite has been attracting growing interest as they exhibit unique electrical, optical and magnetic properties for numerous applications such as oil recover (Natarajan *et al*., 2019), development of drug delivery (Azizi, 2020) as well as electronic and optical devices, and wastewater treatment adsorbents and catalysis (Campos *et al*., 2015; Ruíz-baltazar & Reyes-lópez, 2019). Fe_3O_4 materials not only used for its recyclability also have a very active surface for the adsorption/immobilization of metals and ligands but can prevent the aggregation of metal NPs (Mishra *et al*., 2019). More effectively Ag-Fe_3O_4/g-C_3N_4 nanocomposites catalyst could be recovered by an applied external magnet and reused without the loss of photocatalytic activity which synthesized by hydrothermal methods (Pant *et al*., 2017). However this study used hydrothermal method which has disadvantages such as utilization of organic solvents, harsh reaction conditions (high temperature and pressure) and use of expensive and toxic reducing agents, use of expensive capping agents and organic surfactants, which make them environmentally and economically malignant (Ahmadi *et al*., 2014). Biosynthesis is an inexpensive, faster eco-friendly and nontoxic method for the preparation of the nanoparticles (Sajjadi *et al*., 2017).

In this study, the Ag NPs, Fe_3O_4 NPs and Ag-Fe_3O_4 nanocomposites were synthesized using aqueous extract of *Cymbopogon citratus* leaves as a reducing and capping agent. The Synthesized Ag-Fe_3O_4 nanocomposites decorated with graphitic carbon nitride applied to decompose methylene blue under irradiation with the visible light. The Synthesized nanocomposites also applied to gram-negative and gram-positive bacteria strain and showed excellent result against both bacteria's.

1.2. Statement of the Problem

Due to increased economic activity, mainly in industrial countries, has shown a rise in pollution generated from waste such as sewage, trash, and litter. Particularly, the textile industry produces a significant amount of liquid effluent pollutants due to the vast amounts of water used in fabric processing. Azo dyes like MB dye are the most important source of textile dyes utilized in industrial applications, these result lead to worldwide water pollution. Organic dyes cannot be degraded through the conventional water treatment process due to their complex aromatic structures, hydrophilic nature, and high stability against light, temperature, water, chemicals. And also the majority of bacteria-caused disease is one of the negative impacts of wastewater, and this microbial infection, shows rapid emergence of drug resistance to recent antibiotics, so the development or modification of antimicrobial compounds is alternative treatments. Different conventional methods were used for the reduction of these dye compounds from industrial wastewater. But those approaches are time-consuming, costly, and pose disposal problems.

Heterogeneous photocatalysis is a promising strategy for advanced oxidation environmental remediation. As the previous study reported by Pant et al (Pant *et al*., 2017) Ag-Fe_3O_4/g-C_3N_4 nanocomposite synthesized hydrothermal method and degrade dyes, several chemical and physical methods used for the preparation, so these methods have disadvantages such as the utilization of organic solvents, harsh reaction conditions, and use of expensive reducing agents. The present study synthesized photocatalaytical material with antibacterial properties by green and cost-effective methods.

1.3. Objectives

1.3.1. General Objective

The overall objective of this study is to synthesize and characterize recyclable silver magnetite nanocomposites decorated with graphitic carbon nitride using green method for photocatalytic degradation of dye and antibacterial application.

1.3.2. Specific Objectives

- To Synthesize Fe_3O_4 NPs, Ag NPs, Ag-Fe_3O_4 NC and Ag-Fe_3O_4 NC decorated g-C_3N_4 through green method using aqueous extract of *Cymbopogon citratus* leaves as a reducing agent.
- To characterize the synthesized Ag NPs, Fe_3O_4 NPs, g-C_3N_4, Ag-Fe_3O_4 NC and Ag-Fe_3O_4/g-C_3N_4 NC.
- To investigate photocatalytic degradation efficiency Ag NPs, Ag-Fe_3O_4 NC and Ag-Fe_3O_4/g-C_3N_4 NC against synthetic methylene blue dye.
- To evaluate antibacterial activity of the synthesized nanomaterials using disk diffusion method against selected Gram-negative bacterial strains (*E. coli,* and *P.aeruginosa)* and Gram-positive bacteria (*S. pyogenes* and *S. aureus*)
- To evaluate the recyclability of Ag-Fe_3O_4/g-C_3N_4 NC

1.4. Scope of the Study

The scope of this study was limited to the synthesis of Ag NPs, Fe_3O_4 NPs, and Ag-Fe_3O_4 NC using an aqueous extract of *Cymbopogon citratus* leaves as a reducing agent and preparing g-C_3N_4 by simple calcination from urea. Then the synthesized Ag-Fe_3O_4 nanocomposites were decorated urea-derived g-C_3N_4. The synthesized material was characterized by using UV-Vis spectroscopy, XRD, FTIR, and SEM techniques. The evaluation of the photocatalytic degradation of methylene blue using the synthesized nanoparticles and nanocomposites and its antibacterial activity was performed against representative Gram-negative and Gram-positive bacteria strains.

1.5. Significance of the Study

This study provides important information about the green synthesis strategy of Fe_3O_4 NPs, Ag NPs, Ag-Fe_3O_4 NC, and Ag-Fe_3O_4/g-C_3N_4 nanocomposites by using *Cymbopogon citratus* leaves as a reducing agent and producing g-C_3N_4 which is precious and important material by a simple method and from inexpensive material. This study will help to develop greenly synthesized photocatalysts for the removal and recycle of industrials discharge organic dyes for water environmental remediation. And attempt to fill the gap in eco-friendly, recyclable, and cost-effective synthesis of nanomaterials to remove toxic dyes and antibacterial agents.

CHAPTER TWO

2. Literature Review

2.1. Silver (Ag) Nanoparticles

Silver nanoparticles are a class of materials with sizes in the range of 1–100 nm. The increased interest in the study of Ag NPs is because of their unique attractive physical, chemical, and biological properties (Geetha *et al.*, 2014). Ag NPs are also known to have unique properties in terms of toxicity, surface plasmon resonance, and electrical resistance. Based on these, intensive works have been conducted to investigate their properties and potential applications for several purposes (Syafiuddin *et al*., 2017).The use of silver nanoparticles in different fields of the area is receiving great consideration among researchers in recent years. The physical, chemical and mechanical features of Ag NPs are novel and beneficial in the field of electronics and electrical, biotechnology, Bioengineering, textile engineering, environmental and pharmaceutical (Rauwe *et al.,* 2015). The metal nanoparticles have surface Plasmon resonance (SPR) and its strong observation of light is utilized for the manufacturing of optical devices (Thamilselvi & Radha, 2018). Hence, Ag NPs can be used as a catalyst for a number of chemical transformations because of their excellent activity (Xiao *et al*., 2015). Furthermore, due to the large surface area, the catalytic property of silver nanoparticles can be remarkable as the reaction occurs on the surface (Radhakrishnan, 2018). Silver nanoparticles owing to their powerful bioactivities against bacteria, fungi, protozoa, and viruses have been considered the most promising antimicrobial agents among other metals nanoparticles (Gupta & Ganjewala, 2015).

2.1.1. Synthesis Methods of Silver Nanoparticles

Nowadays several methods and, approaches have been reported for the synthesis of Ag NPs by using chemical, physical, photochemical and biological routes. Each method has advantages, and disadvantages with current problems being costs, scalability, particle sizes and size distribution, and so on (Natsuki *et al*., 2015). Synthesis using chemical approaches incorporating, chemical reduction, photochemical method, electrolysis and ultrasonic spray pyrolysis are some examples of chemical synthesis methods. Physical methods includes, vapor

condensation, arc discharge, laser ablation and physical deposition also used to synthesize nanoparticles (Yusuf, 2019).

These methods have resulted in superior NPs but still a key understanding of improved manufacturing process is required which could be exploited at the industrial and commercial level to have better built, long lasting, cleaner, safer and smarter products such as home appliances, communication technology, medicines, transportation, agriculture and industries (Gamboa *et al*., 2019). Additionally, metal nanoparticles have high surface energy making them less stable. Therefore, resulting nanoparticles aggregate and prefer to obtain more stable morphology, such as a truncated triangle to minimize their Gibbs free energy (Mohammadlou *et al*., 2016). Many adverse effects have been also associated with chemical and physical synthesis methods due to the presence of some toxic chemical absorbed on the surface (Hasan, 2015). Therefore, the recent studies main focus is to design NPs using environmentally benign approaches. These provide solutions to growing challenges related to environmental issues (Sharma *et al*., 2019). Nature has designed to contribute ways and insight to the synthesis of advanced nanomaterials. In chemistry and chemical technology environmentally friendly synthesis methods are becoming more and more popular (Protima *et al*., 2015). The green synthesis of silver nanoparticles approach has triggered use of different sources, like bacteria, fungi, algae, and plants, resulting in large-scale production with less contamination. Green synthesis is an eco-friendly and biocompatible process, generally accomplished by using a capping agent/stabilizer (to control size and prevent agglomeration), plant extracts, yeast, or bacteria (Shabina *et al*., 2020). A biosynthetic protocol is usually a three-step procedure. The first is the selection of a benign solvent medium for the synthesis such as lower alcohols and water. Secondly, the selection of a benign reducing agent, for those processes that require a precursor reduction, must preferably encourage the use of biological metabolites possessing an adequate oxidizing potential so that nanoparticle precursor can be reduced to its metallic state. Finally, the biological substrate must contain metabolites that act as capping agents and promote the stabilization of the nanoparticles (Jacinto *et al*., 2021).

Usually considering environmental concerns for the synthesis of Ag NPs, the green approach is preferred over current methodologies. The conventional synthetic methods for Ag NPs need a huge amount of energy and hazardous chemicals and may lead to the formation of dangerous byproducts (Ajayi & Afolayan, 2017). The use of biodegradable polymers, sugars, or

polyphenols from plant extracts, enzymes, and bacteria under ambient circumstance may lead to the sustainable synthesis of Ag NPs with a uniform size. Ag NPs formed in more basic pH (>11) are stable and in acidic pH (<7) are unstable and agglomerated (Tarannum & Gautam, 2019). The size, shape, in general, the morphology of the nanoparticles are dependent on the specific control of factors such as reaction kinetics, temperature, pH, etc., so that the synthesis method is particular in achieving the nanoparticle that is sought to be synthesized. Additionally, the precursor of Ag NPs also have factors, the vast majority used Silver Nitrate which is recrystallized and purified to be used as precursors of silver nanoparticles (Gamboa *et al.,* 2019).

2.1.1.1. Synthesis via Plant Material

Various parts of plant such as leaves, roots, flowers, fruits, rhizomes *etc.*, have been effectively utilized for the synthesis of Ag NPs. Different parts of plant are collected from various sources, washed properly with ordinary water followed by distilled water to exclude debris and any other unwanted materials (Vanlalveni *et al*., 2021). After that, the portions are dried and ground to make powder or utilized as fresh to make the extract. To prepare the extract, the chopped pieces or the ground powder of the parts of the plant are put in deionized water or alcohol and usually heated below 60°C for few hours as high-temperature heating long time may leads to the decomposition of phytochemicals in the biomass extract (Alabdallah & Hasan, 2021). Plant extract of different pH is added to the solutions having a different concentration of Ag salt as metal precursor followed by heating at different temperature led to the synthesis of Ag NPs (Sajid & Płotka, 2020). This synthesis process avoids the use of chemical stabilizer as biomaterials present in the extract act as a reducing agent as well as a stabilizing agent for the synthesis of Ag NPs (Vanlalveni *et al*., 2021). Various plant metabolites, including terpenoids, polyphenols, sugars, alkaloids, phenolic acids, and proteins play an important role in the bioreduction of metal ions to form nanoparticles (Mohammadlou *et al*., 2016). Different study reported that Ag NPs has been synthesized using various Plant such as *Cinnamon camphora*, *Eucalyptus camaldulensis* (Emad *et al*., 2009), *Geranium* (Shankar *et al*., 2003), *Azadirachta indica* (Shankar *et al*., 2004), *Aloe vera* (Chandran *et.al*., 2006), *Tamarindus indica* (Ankamwar *et al*., 2005), *Acalypha indica* (Krishnaraj *et al*., 2010), *Pongamia pinnata* (Rajesh *et al.*, 2010) and *Cymbopogon citratus* (Geetha *et al*, 2014).The development of these eco friendly or using

plants for the synthesis of nanoparticles is evolving into an important branch of nanotechnology for silver nanoparticles, which have many applications and effective (Hasan, 2015).

2.1.1.2. Synthesis via Microorganisms

The utilization of microorganisms like fungi, yeasts, bacteria and algae, are important nano-factories that can accumulate and detoxify heavy metals due to the presence of various reductase enzymes that can reduce metal salts to MtNPs (Bahrulolum *et al*., 2021). When metal NPs were synthesized outside the cells, the extracellular components acted as dispersants; dispersant-capped metal NPs were not aggregated and, the metal NPs synthesized outside the cells were zero-valent metals, the extracellular components and added electron donor or membrane components acted as reductants. However, when metal NPs were synthesized inside the cells, proteins or peptides acted as dispersants (Kato & Suzuki, 2020). For intracellular synthetic procedure microorganisms are cultured in a suitable growth medium with favorable pH and temperature conditions (Prasad, 2019). The biomass is harvested after an optimal incubation period and washed thoroughly with sterile water to minimize potentially undesirable effects of the culture medium. The resulting biomass is then incubated with the metal salt solution. The extracellular biosynthesis of MtNPs is carried out by trapping metal ions on the cell wall and reducing them in the presence of secreted enzymes or metabolites. In the intracellular biosynthesis of MtNPs, after the transfer of metal ions into the cell cytoplasm, the metal ions are reduced as a result of metabolic reactions with enzymes, such as nitrate reductase (Bahrulolum *et al.,* 2021).

2.1.2. Silver Nanoparticles as Photocatalyst

Among the nanomaterials, metal nanoparticles such as Ag NPs gained abundant attention in the scientific regime and industrial field because of their imperative physical, chemical, and optical properties (Ijaz *et al*., 2020). As the silver nanoparticles have an exceptional property to absorb the visible and UV light from solar irradiations due to the surface plasmon resonance (SPR) effect. Thus, they have prodigious potential to combat noxious dyes through an effective photocatalytic process. Therefore, the practical implementation (e.g., operation under visible light) of nanostructures-based photocatalyst (e.g., Ag NPs) should be one of the most effective and preferable system to treat noxious organic pollutants (Singh *et al.,* 2019). As

Figure 1 indicates silver nanoparticle has potential to convert dye molecules into non-toxic products by photocatalytic process. Ag NPs possess considerable photocatalytic activity and when they are impregnated in a less active material, labeled catalytic support, toxicity issues can be fixed (Qi *et al*., 2020).

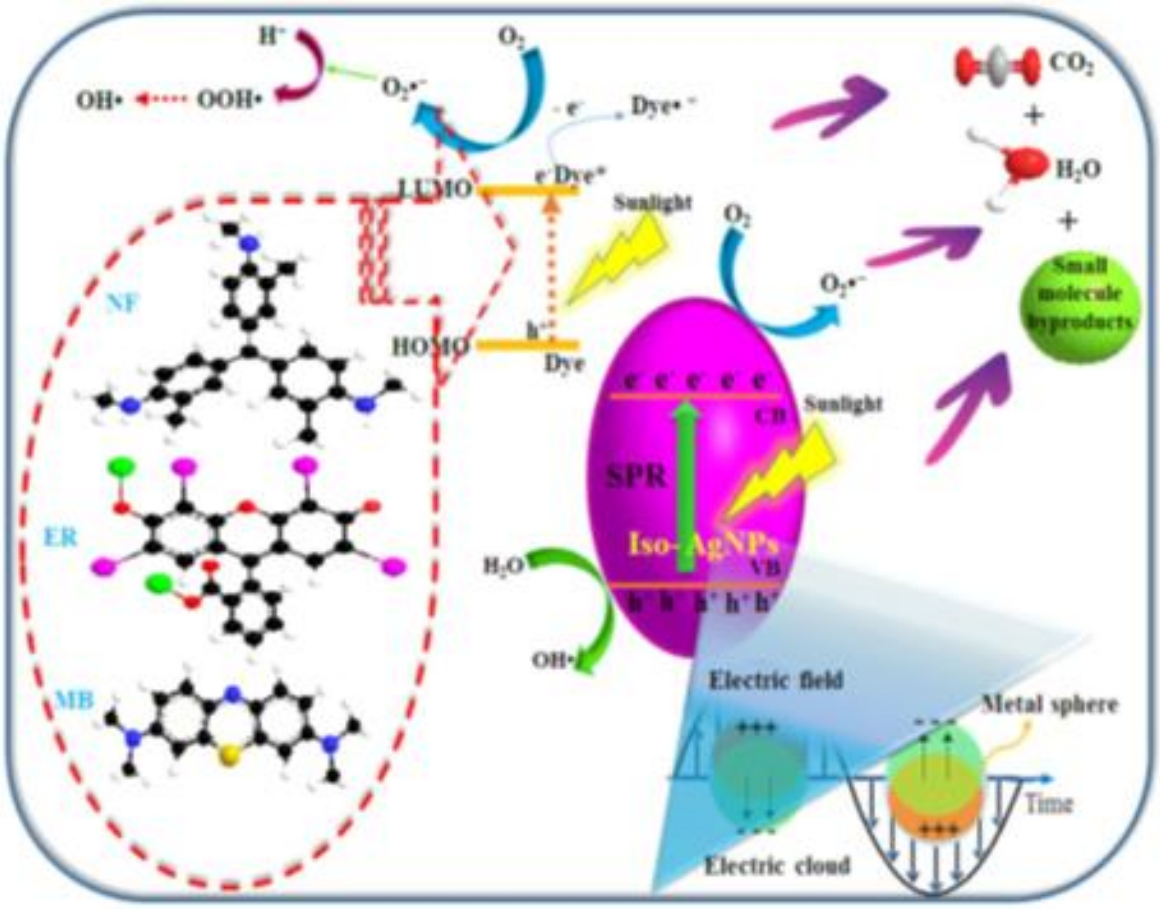

Figure 1. Photocatalytic degradation mechanism of dyes using Ag NPs proposed by (Mavaei *et al*., 2020)

2.1.3. Silver Nanoparticles as Antibacterial Agent

Silver is easily available and is known to have an antimicrobial effect; moreover, it does not impose any adverse effects on the human body. Nanosilver is used as an antimicrobial agent; it is employed in textiles, home water purification systems, medical equipments, cosmetics, electronics, and household appliances (Mathur *et al*., 2018). The antimicrobial effect is mainly due to silver ions, which have a broad antibacterial spectrum. Moreover, the development of

multidrug-resistant bacteria, as in the case of antibiotics, is less likely (Nakamura *et al*., 2019). The silver nanoparticles are bringing much interest because of their vigorous antibacterial activity. Researchers have also shown an important activity of silver nanoparticles against bacterial biofilms (Franci *et al*., 2015). The antibacterial effect is due to their formation of free radicals on its surface to penetrate through the membrane of the cell to interrupt the intracellular processes. Ag NPs can physically interact with the cell surface of various bacteria. This is particularly important in the case of Gram-negative bacteria where numerous studies have observed the adhesion and accumulation of Ag NPs to the bacterial surface. Recent studies have reported that Ag NPs can damage cell membranes leading to structural changes, which render bacteria more permeable and Ag NPs more effective against *E. coli* than against *S.aureus* (Roy *et al*., 2019). Current studies suggest that the biosynthesized Ag NPs have effective antimicrobial potential and could serve as an alternative to developing an antimicrobial compound to solve the problem of drug resistance.

The privies review (Durán *et al*., 2016) on the antibacterial activity of silver nanoparticles stated that silver nanoparticles did not significantly exert direct particle-specific toxicity on bacteria as Figure 2 demonstrate serve as a carrier to more effectively deliver silver ions to the bacteria cytoplasm and membrane. As Figure 2 shows silver nanoparticles kill bacterial cells in various mechanisms. Onaway through which bacteria killed by Ag NPs is disruption of the cell wall and cytoplasm, and by denaturation of ribosomes: silver ions denature ribosomes and inhibit protein synthesis (Mathur *et al*., 2018). Interruption of adenosine triphosphate (ATP) production: ATP production is terminated because silver ions deactivate respiratory enzyme on cytoplasm membrane and membrane disruption by reactive oxygen species: reactive oxygen species produced by the broken electron transport chain can cause membrane disruption is the another way (Dakal *et al*., 2016). Interference of deoxyribonucleic acid (DNA) replication: silver and reactive oxygen species bind to deoxyribonucleic acid and prevent its replication and cell multiplication and perforation of membrane: silver nanoparticles directly move across cytoplasmic membrane, which can release organelles from cell (Yin *et al*., 2020; Durán *et al*., 2016). Based upon the previous discussion it can be said that the synthesis of nanoparticles may serve as a future direction in biomedical nanotechnology in developing antibacterial compound.

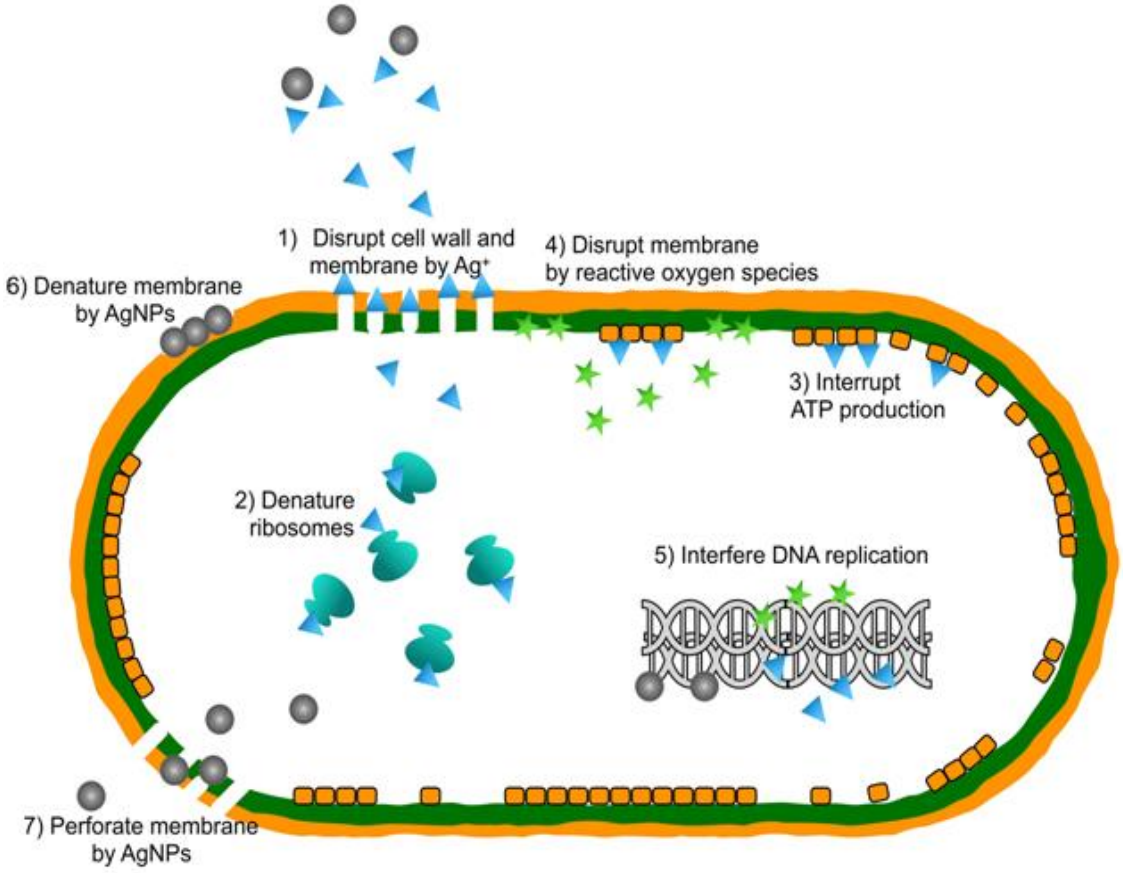

Figure 2. The antibacterial actions of silver nanoparticles proposed by (Yin *et al*., 2020)

2.2. Magnetite (Fe_3O_4) Nanoparticles

Fe_3O_4 is obtained from various sources such as black iron oxide, magnetic iron ore, loadstone, ferrous ferrite and Hercules stone. There are eight different iron oxides that are well known in nature, among them magnetite and maghemite (Fe_3O_4), (γ-Fe_2O_3) and hematite (α-Fe_2O_3) shows the unique magnetic properties and they have different polymorphic forms and undergo temperature induced phase transition (Gangadhar *et al*.,2021). Magnetite and maghemite are excellent materials for industrial and biomedical applications. Both have a reusable advantage over other iron oxides due to their unique magnetic, catalytic and biochemical feature (Natarajan *et al*., 2019). Fe_3O_4 has faced centered cubic spinel structure with both divalent and trivalent iron in it. All of the Fe^{2+} ions reside in half of the octahedral sites whereas the Fe^{3+} ions are divided evenly across the remaining available octahedral and the tetrahedral sites (Cornell & Schwertmann, 2003; Mohapatra & Anand, 2010).

Magnetite minerals can exhibit the strongest magnetism amongst other phases of iron oxides. Typically, the natural magnetite with a density of 5.2 g/cm3 can be found as fine grains in sedimentary rocks with hardness of 5.5 to 6.5 on Mohs scale (Torres *et al*., 2009). Magnetite has been attracting growing interest as they manifest novel electrical, optical and magnetic properties for various purpose such as generation of inorganic pigments, magnetic storage media, development of gas sensors as well as electronic and optical devices, information storage, color imaging, magneto caloric refrigeration, bioprocessing, ferrofluid technology and wastewater treatment adsorbents (Campos *et al*., 2015). Metal nanoparticles with high magnetic characteristics, including nickel and cobalt, but they are easily oxidized, and toxic (Natarajan *et al*., 2019). Magnetite (Fe_3O_4) is the most magnetic naturally occurring material containing both $Fe^{3+}$and Fe^{2+} ions in a 2:1 stoichio-metric ratio. Due to its magnetic properties, magnetite nanoparticles is used in water purification agents, high-density magnetic data storage media, and magnetically recoverable catalysts (Mirabello *et al.*, 2016).

2.2.1. Synthesis Approaches of Fe_3O_4 Nanoparticles

Several conventional approaches including co-precipitation and thermal decomposition are extensively employed for MNPs synthesis. The co-precipitation method is used due to its integrity whereas thermal decomposition is a good method in controlling nanoparticle size and morphology. Those techniques use chemicals as a reagent that are not environmentally friendly (Mohamad *et al.*, 2017). The most popular method used to synthesize Fe_3O_4 is through co-precipitation of ferrous (Fe^{2+}) and ferric (Fe^{3+}) aqueous salt solutions by using an alkali such as sodium hydroxide (NaOH) or ammonium hydroxide (NH_4OH). The co-precipitation process involves the precipitation of iron precursors Fe^{2+} and Fe^{3+} at a molar ratio of 1:2. (Ling *et al*., 2016).

The chemical co-precipitation can be expressed as

$$Fe^{2+} + 2Fe^{3+} + 8OH \rightarrow Fe_3O_4 + 4H_2O$$ ..... Equation 1

There are a lot of successful studies where Fe_3O_4 NPs can be synthesized using different biological routes, however, the plant extract is the most widely used in green synthesis because it can be obtained easily, large-scale production, cost-effective and environmental benign (Viju & Prem, 2018). Different plants are used for synthesis of magnetite, lemongrass (*Cymbopogon sp)* (Hiremath *et al*., 2018), *Graptophyllum pictum* leaf (Sari & Yulizar, 2017)

and Chromolaena odorata root etc..(Nnadozie & Ajibade, 2020). In green synthesis of Fe_3O_4 NPs, firstly, a solution of Fe^{3+} and Fe^{2+} with a 2:1 M ratio mixed with plant extract NaOH or base added to the solution to adjust the pH 11. Also the solution stirred to homogenize the solution and also for the completion of reaction. After that, the as-synthesized Fe_3O_4 NPs separated by using a magnet (Yew *et al*., 2016).

2.2.2. Magnetite (Fe_3O_4) Nanoparticles as Photocatalyst

Magnetite NPs are well renowned for its easy recovery, ease of handling and catalytic activity for various applications. It is well known that the iron oxide nanoparticles have renowned photocatalytic activity by the virtue of their low band gap, more stableness, high surface area and good light absorption capacity (Ganapathe *et al*., 2020). Fe_3O_4 NPs system may be attributed to the rapid transfer of the photo-generated electrons resulting in the effective separation of the electrons and holes. Hole itself is a strong oxidant that can oxidize the OH^- and H_2O that are adsorbed on the Fe_3O_4 surface, yielding the HO^- free radical. The HO^- radical adsorbed on Fe_3O_4 surface is a strong oxidant and it not only oxidizes the organic compound adsorbed, but also diffuses into the bulk solution and oxidizes the organic compounds (Xuanxuan *et al*., 2017). Nanosized magnetic Fe_3O_4 used as a photocatalyst for the degradation of azo dyes, such as methyl red and Congo red (Natarajan *et al*., 2019).

2.2.3. Magnetite (Fe_3O_4) Nanoparticles for Antibacterial

Magnetite NPs have been used in recent antibacterial studies as an increasingly more research area. A number of microorganisms exist in the size scales from nanometer to micrometer regions. Many biocompatible MNPs have been introduced that possess remarkable impacts against various drug- resistant bacteria strains (Allafchian & Hosseini, 2019). As Figure 3 indicates, one of the main mechanisms of IONP toxicity is ROS generation, including in photocatalysis, Fenton reactions. ROS, in turn, have a genotoxic action, damaging DNA molecules. An increase in ROS concentration can be caused by a decrease in the activity of antioxidant system enzymes (SOD, catalase, and glutathione reductase). Metal ions can bind mecapto (–SH), amino (–NH), and carboxyl (–COOH) groups of proteins, including enzymes, which leads to inactivation or partial inhibition (Gudkov *et al.*, 2021).

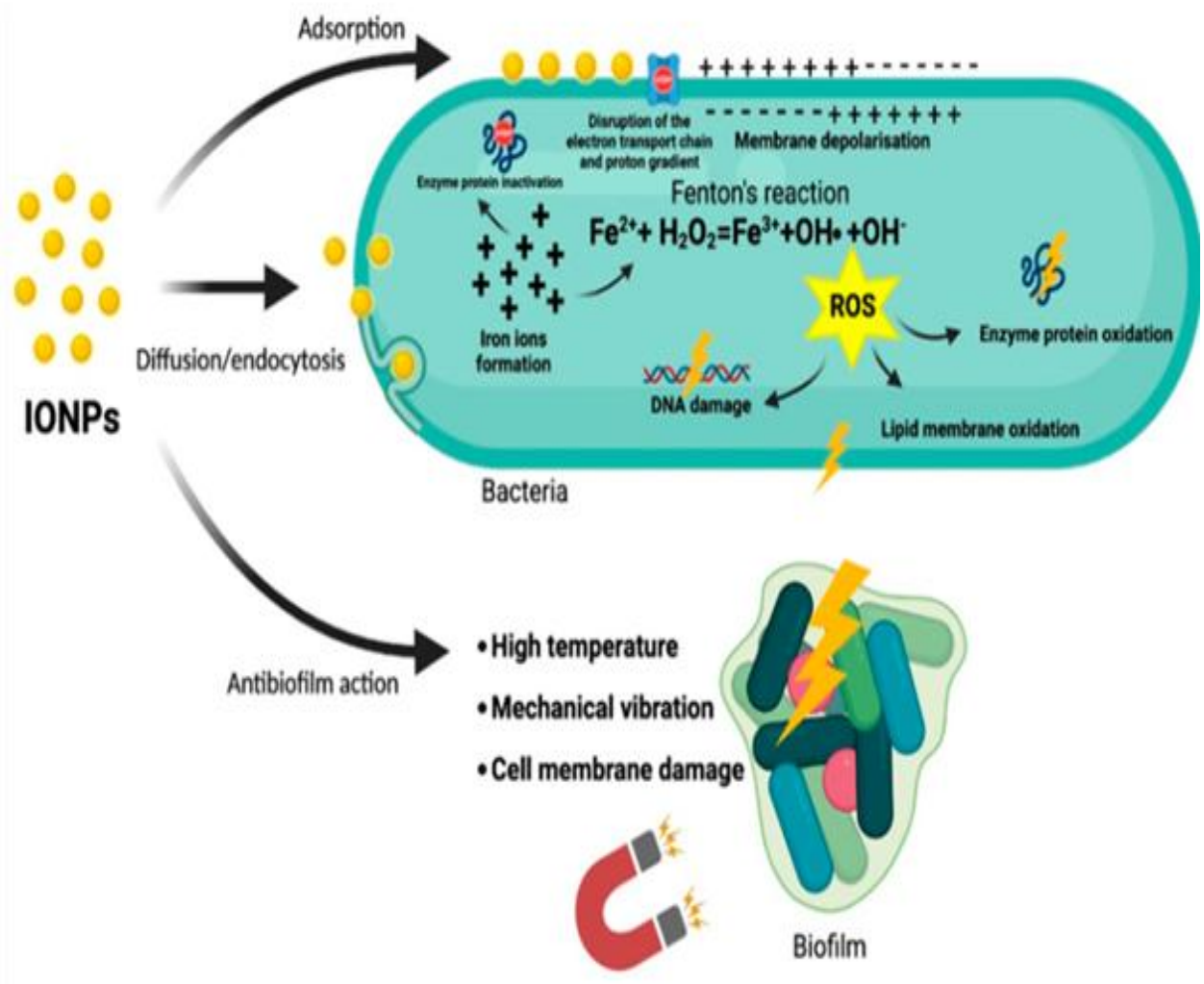

Figure 3. The antibacterial action of magnetite nanoparticles (Gudkov *et a*l., 2021).

2.3. Graphitic Carbon Nitride

Graphitic carbon nitride is one of the oldest artificial polymers reported back in 1834. Structurally analogous to graphene, this conjugated polymer is novel, metal free with a medium band gap of 2.7 eV. Generally, there are different allotropes of C_3N_4 such as α-C_3N_4, β-C_3N_4, pseudocubic C_3N_4, cubic C_3N_4, g-h triazine and g-C_3N_4. However, g-C_3N_4 is considered the most stable form of C_3N_4 under ambient condition (Fakhrul *et al*., 2003). Figure 4 demonstrate the basic tectonic units to establish the allotropes of the g-C_3N_4 photocatalyst. The tri-s-triazine-based g-C_3N_4 photocatalyst is the most stable phases of C_3N_4 at ambient condition (Zheng *et al*., 2016).

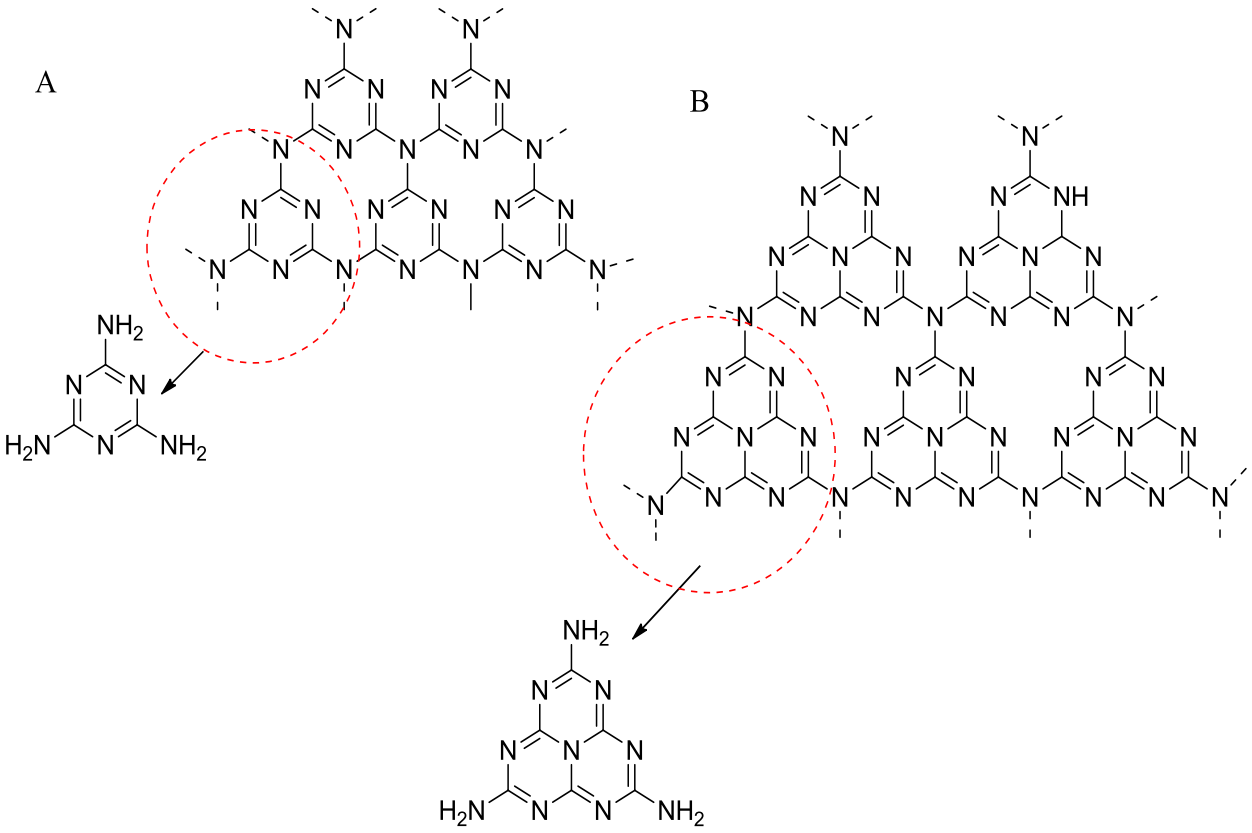

Figure 4. The molecular structure of the basic tectonic units for g-C_3N_4, ($A_)$ triazine and (B) tri-s-triazine (B).

2.3.1. Preparation Methods of Graphitic Carbon Nitride

Graphitic carbon nitride (g-C_3N_4) can be prepared by the thermal decomposition of various carbon and nitrogen-rich organic precursors in a controlled atmosphere. There are different methods to synthesize g-C_3N_4, which in general require high temperatures. Among these methods, pyrolysis is a relatively simple method that requires no additive other than the precursor itself (Fakhrul *et al*.,2003). The urea-derived graphitic carbon nitride samples prepared achieved degradation efficiencies of greater than melamine derived graphitic carbon. Graphitic carbon nitride (g-C_3N_4) was successfully prepared using different precursors, melamine and urea (Fakhrul *et al.*, 2003), thiourea, and dicyandiamide at the same conditions (Zhao *et al*., 2017). Graphitic carbon nitride (g-C_3N_4) prepared by a one-step method at calcination. Typically, the reagent in covered crucible calicnated in a muffle furnace, different pyrolysis temperatures (500, 550, 600 and 650°C) (Liu *et al*., 2020).

2.3.2. Graphitic Carbon Nitride as Photocatalyst

Considerably, reaping of visible light, mostly from sunlight, by catalyst (photocatalyst) to initiate chemical transformations is described as photocatalysis. The application of C_3N_4 photocatalyst for wastewater treatment, solar energy utilization, environmental treatment, and biomedical and sensing applications has been discussed in many areas of science (Gao and Zhang, 2020). Due to these exceptional properties of g-C_3N_4, the use of this promising g-C_3N_4 in water splitting, CO_2 photoreduction, organic contaminants purification, catalytic organic synthesis, and fuel cells is more efficient and effective (Zheng *et al*., 2016). Carbon derivatives such as activated carbon exfoliate graphite, graphene oxide, graphene, carbon nanotubes are the conventional material widely reported for water treatment and sensor applications. Graphitic carbon nitride (g-C_3N_4) an effective material to remove and sensing of the contaminated wastewater containing dyes and 81 pharmaceutical products is reported by several reports utilizing photocatalysis and electrochemical sense (Mohanraj *et al*., 2020; Nafisa *et al.*, 2019). This compound possesses excellent visible light absorption than most of the metal oxide photocatalyst owing to its mild bandgap energy. Given its p-conjugated properties, g-C_3N_4 can act as an electron sink, leading to the suppression of recombination of photo-excited charge carriers (Kong *et al*., 2021). Moreover, the polymeric nature of this material allows for multiple excitations from absorption of a single photon, leading to an efficient generation of the reactive species responsible for pollutant degradation as illustrated in Figure 5.

Figure 5. Phocatalytical degradation mechanism of g-C_3N_4 (Geo and Zhang, 2020)

As illustrated in Figure 5 In a single 2D g-C_3N_4 system, the photo-excited electrons of the conduction band (CB) generally return to the valence band (VB), while the unpopular recovery of photo-generated electrons and holes are a great disadvantage of photocatalytic reactions. The photocatalyst is used as a semiconductor, to intimately constitute with g-C_3N_4, to create a suitable band structure (Xiao *et al*., 2015).

2.3.3. Antibacterial Application of Graphitic Carbon Nitride

Generally, 2D materials have been reported to exhibit certain intrinsic antibacterial properties without exogenous excitation because of their unique 2D nanosheet structure (Xin *et al*., 2019). Their sharp edges can physically cut bacteria directly like a knife, causing cellular dysfunction and leakage of cytoplasmic components through the destruction of bacterial cell walls and membranes. These can be confirmed by scanning electron microscopy images or measuring the release of bacterial intracellular components, such as bacterial RNA, ATP, and proteins (Kong *et al*., 2021; Zou *et al*., 2016). As shown in Figure 6 cell rupture of bacteria caused by direct mechanical contact between g-C_3N_4 nanosheet and cell membrane are observed.

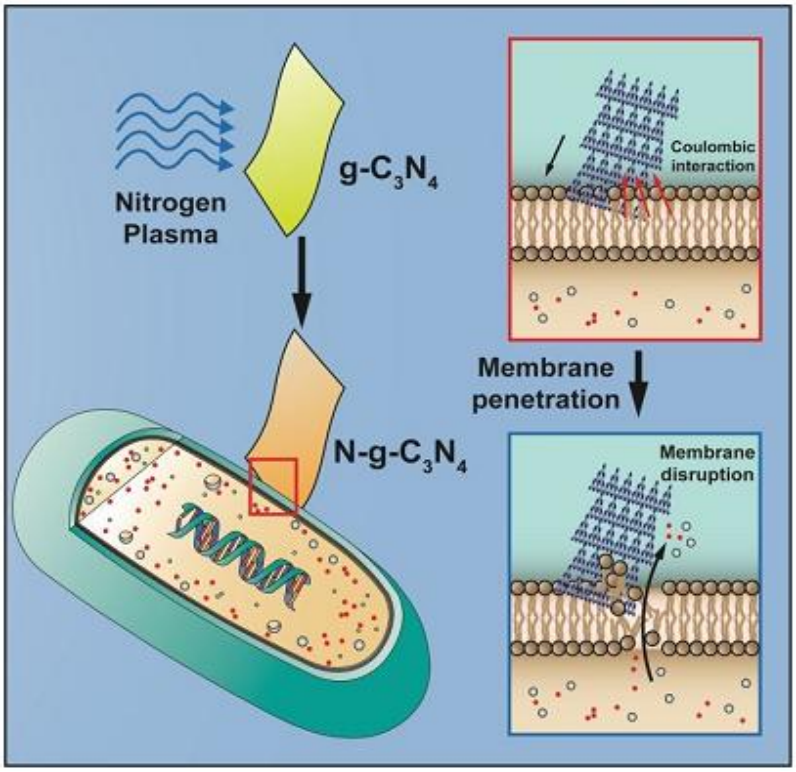

Figure 6. The physical bacteria-killing effect caused by g-C_3N_4 (Marimuthu *et al*., 2020)

2.4. Ag-Fe_3O_4 /g-C_3N_4 Nanocomposites

Nanocomposites are the heterogeneous/hybrid materials that are produced by the mixtures of polymers with inorganic solids (clays to oxides) at the nanometric scale. They attract much attention because of their enhanced potential applications in many fields including optics, electrics, magnetism, ceramics, and hetrocatalysis (Said *et al*., 2020).

2.4.1. Synthesis of Ag-Fe_3O_4 /g-C_3N_4 Nanocomposites

The Ag-Fe_3O_4/g-C_3N_4 nanocomposites have been prepared by a simple one-step hydrothermal technique. In hydrothermal synthesis, the formation of nanomaterials can happen in a wide temperature range from room temperature to very high temperatures. To control the morphology of the materials to be prepared, either low-pressure or high-pressure conditions can be used depending on the vapor pressure of the main composition in the reaction (Gan *et al*., 2020). The synthesized g-C_3N_4 dispersed an aqueous solution by ultrasonication. Then magnetite, and silver source and PVP added and subjected to the stirring. Finally, cooled to room temperature and then obtain product (Nguyen *et al*., 2020).

2.4.2. Photocatalaytical Application of Ag-Fe_3O_4 /g-C_3N_4 Nanocomposites

Thus, the composites of Ag NPs, Fe_3O_4 NPs, and g-C_3N_4 show the functions of all components and can be applied effectively in wastewater treatment. There are several reports for the preparation of magnetically separable and visible-light-driven photocatalyst based on g-C_3N_4 (Amarjargal *et al*., 2013; Wang *et al*., 2016). The recent report on the magnetically separable Ag/Fe_3O_4/g-C_3N_4 photocatalyst has multiple applications such as hydrolysis of ammonia borane to liberate H_2 gas, removal of organic dyes from aqueous solution, and antibacterial investigations.

Ag/Fe_3O_4/g-C_3N_4 nanocomposites exhibited a strong photocatalytic activity for the decomposition of methyelen blue and hydrolysis of the ammonia–borane (Pant *et al* , 2017). Ag-Fe_3O_4/g-C_3N_4 nanocomposites significant photocatalytic degradation in methyelen blue (MB) dye, the hydrogen evolution rate by hydrolysis of ammonia-borane (AB). More importantly, the as-synthesized silver iron oxide nanoparticles decorated graphitic carbon nitride (Ag-Fe_3O_4/g-C_3N_4) nanocomposites catalyst could be recovered by an applied external magnet and reused without the loss of photocatalytic activity (Pant *et al.*, 2017).

2.4.2.1. Heterogeneous Photocatalysis

Heterogeneous photocatalysis is a discipline which includes a large variety of reaction: mild or total oxidations, dehydrogenation, hydrogen transfer, oxygen-18 and deuterium isotopic exchange, metal deposition, water detoxification, gaseous pollutant removal, bacterial action etc (Herrmann, 2005).

As for classical heterogeneous catalysis, the overall process can be decomposed into five independent steps: Eley-Rideal (E-R) mechanism, (Langmuir-Hinshelwood, Mars van Krevelen and Eley Rideal) (Saeed *et al*., 2018)

1. Transfer of the reactants in the fluid phase to the surface
2. Adsorption of at least one of the reactants
3. Reaction in the adsorbed phase
4. Desorption of the product(s)
5. Removal of the products from the interface region

Heterogeneous photocatalysis can be defined as the acceleration of a photoreaction in the presence of a catalyst. Moreover, it is inexpensive; can be carried out under ambient conditions (Mekdes, 2021). Compared to homogeneous transition metals for activation, the heterogeneous systems have several advantages with respect to the recovery of catalysts, decrease in the secondary pollution and lower need for catalysts' amount (Wang, 2019).

Among the various nanocomposites, ZnO/CuO (Mekdes, 2021), Fe_3O_4–Ag nanocomposites (Khaghani & Ghanbari, 2016) and $Ag/AgFeO_2$ decorated on g-C_3N_4 nanosheet(Nguy *et al.*, 2020) are some examples of hetronanocatalysts.

2.5. Characterizations of Nanoparticles

Characterization of noble metal nanoparticles for various applications is current areas of research. Strategies used for their fabrication and characterization are going to be improved day by day. Control over size and shape of nanoparticles is very important for their potential applications in various fields (Begum *et al*., 2018).The characterization of nanomaterials before their use is very important in many fields. The characteristics of nanomaterials determine their properties. Surface characterization of nanomaterials is also determined by various techniques. The common methods used for the characterization of nanoparticles

include, ultraviolet visible (UV–Vis) spectroscopy , scanning electron microscopy (SEM), transmission electron microscopy (TEM), low energy electron diffraction (LEED), extended X-ray absorption fine structure (EXAFS) used for the detection of surface topography, and secondary ion mass spectroscopy (SIMS), auger electron spectra (AES), electron probe microanalysis (EPMA) etc (Mohammadlou *et al*., 2016 ; Mourdikoudis *et al*., 2018). Each technique has its own advantages and disadvantages and it is hard to compare one technique to another because each technique has a specific purpose and used to get a specific information that cannot be obtained from the other one (Begum *et al*., 2018).

2.5.1. Ultraviolet Visible Spectroscopy

UV-Vis spectroscopy refers to absorption spectroscopy in the UV-Vis spectral region. Light wave lengths in the 300–800 nm are generally used for characterizing various metal nanoparticles in the size range of 1 to 100 nm (Ijaz *et al*., 2020). Absorption of the UV radiations results in the excitation of the electrons from the ground state to a higher energy state. Generally, the most favored transition is from the highest occupied molecular orbital to the lowest unoccupied molecular orbital. Such electron transfer processes may take place in transition metal ions (d-d transitions and ligand-to-metal or metal-to-ligand charge transfer transitions) and inorganic and organic molecules (mainly π-π* and n-π* transitions). This absorption spectroscopy uses electromagnetic radiation between 190 and 800 nm and is divided into the UV (190-400 nm) and visible (400-800 nm) regions. Because the absorption of UV or visible radiation by a molecule leads to transition among electron energy levels of the molecule, it is also often called electronic spectroscopy (Chirayil *et al*., 2017).

2.5.2. Fourier Transform Infrared Spectroscopy

Fourier Transform Infrared, the preferred method of infrared (IR) spectroscopy. In IR spectroscopy, IR radiation is passed through a sample. Some of the IR radiation is absorbed by the sample and some of it is passed through (transmitted). The resulting spectrum represents the molecular absorption and transmission, creating a molecular fingerprint of the sample. As two finger prints never match, similarly no two unique molecular structures produce the same IR spectrum (Dutta, 2017). A common approach to exploit the unique properties of nanoparticles and to improve its workability is to functionalize the surface of the latter. However, the application of FTIR in the characterization of functionalized nanoparticles could

be difficult because it may not reveal the chemical bonds between the nanoparticles and the functional molecules based on a database of known vibration frequencies. This is because the chemical bond between the functionalized molecules and the nano-material is usually novel, and thus, a strategy must be developed in order to provide evidence about the resonant vibration information between the grafted molecules and the nano-sized particles (Baudot *et a*l., 2010). Biomolecules those are responsible for capping, reduction and stabilizer, are identify by using FT-IR (Ijaz *et al*., 2020).

2.5.2. X -Ray Diffraction

XRD is used for the determination of crystal structure, calculation of crystalline nanoparticles size and for confirmation of nanoparticles (Ijaz *et al*., 2020).

The crystalline structure of nanoparticles can be calculated by using Debye Scherrer s equation (Yang *et al*., 2016).

$$D = \frac{0.9.4\lambda}{\beta Cos\theta} \quad \text{..... Equation 2}$$

It provides information on structures, phases, preferred crystal orientations (texture), and other structural parameters, such as average grain size, crystallinity, strain, and crystal defects. XRD peaks are produced by constructive interference of a monochromatic beam of X-rays scattered at specific angles from each set of lattice planes in a sample. The peak intensities are determined by the atomic positions within the lattice planes. An online search of a standard database for X-ray powder diffraction patterns enables quick phase identification for a large variety of crystalline samples (Thurston *et a*l., 2017).

2.5.4. Scanning Electron Microscope.

Output image is formed by using SEM in which electron is used instead of light. Shape, size, morphology and distribution of synthesized nanoparticles are characterized by using SEM (Ijaz *et al.*, 2020).The characterization of Scanning electron microscope analysis is employed to determine the size, shape & morphologies of formed nanoparticle SEM gives high resolution images of the surface of a sample is desired. The scanning electron microscope works as same principle as an optical microscope, but it measures the electrons scattered from

the sample rather than photon. Because electrons can be accelerated by an electric potential, the wavelength can be made shorter than the one of photons. This makes the SEM capable of magnifying images up to 200.000 times. Measures the particle size and characterization, Conductive or sputter coated sample involved and the sensitivity down to 1nm (Kaur & Kaur, 2019)

2. 6. *Cymbopogon* citratus (Lemongrass leaf)

Cymbopogon citratus is well-known as a lemongrass plant, which grows in tropical and semi-tropical zones of Asia, Africa, Central and South America (Patiño *et al*., 2020) and one of the essential oil-bearing perennial grasses belong to Poaceae or Gramineae family which mainly used for aromatic and medicinal purposes (Meskelu, 2019).

Figure 7. Image of *Cymbopogon citratus* leaf (Geetha *et al*, 2014)

Cymbopogon citratus an economically valuable medicinal plant studies indicate that this plant have bioactive compounds such as Phenolic compound, carbohydrate, Saponin, Steroid, Tannin, Flavonoids, Glycosides, Terpenoids, and Alkaloids (Basera *et al*., 2019). *Cymbopogon citratus* contains, Terpenes, alkaloids (*N*-containing compounds) and phenolics constitute the largest groups of secondary metabolites (Promila, 2020).The above Figure 8

shows some list of terpenes, flavonoids which used as reducing agents found in *Cymbopogon citratus* leaf.

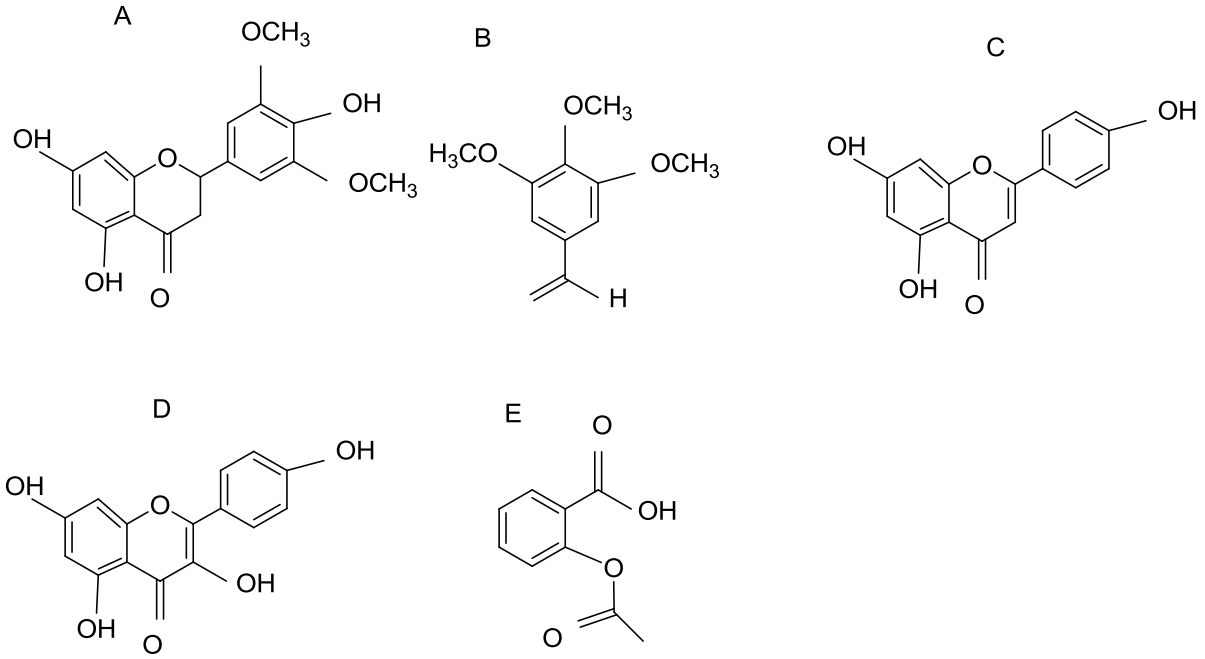

Figure 8. Flavonoids and triterpenoids from Cymbopogon species

Studies have indicated the successful use of *Cymbopogon* extracts for the fabrication of metallic NPs like silver, gold, copper, cerium dioxide, and magnetite which have demonstrated their antibiosis and dye degradation benefits (Geetha *et al*., 2014;Cherian *et al*., 2020)
Therefore, *Cymbopogon citratus* is a promising alternative for the reduction of the metal and metal oxide precursor, allowing the formation and stabilization (Cherian *et al*., 2020).

2.7. Removal of Methylene Blue

Dyes are chemicals which on binding with the material will give color to them. Dyes are also categorized as non-ionic and ionic (e.g., cationic (basic) and anionic (reactive, acid, direct) dyes). methylene blue (MB) is a model cationic dye employed by industries such textile industry for a variety of purposes such as in coloring paper, dyeing cotton, wools, silk, leather, and coating for paper stock (Aragaw *et al*., 2020). It has molecular formula $C_{16}H_{18}N_3SCl$ (3,

7-bis (dimethylamino)-phenothiazin-5-ium chloride) or Tetra methylene blue, the chemical structure is present in Figure 9A

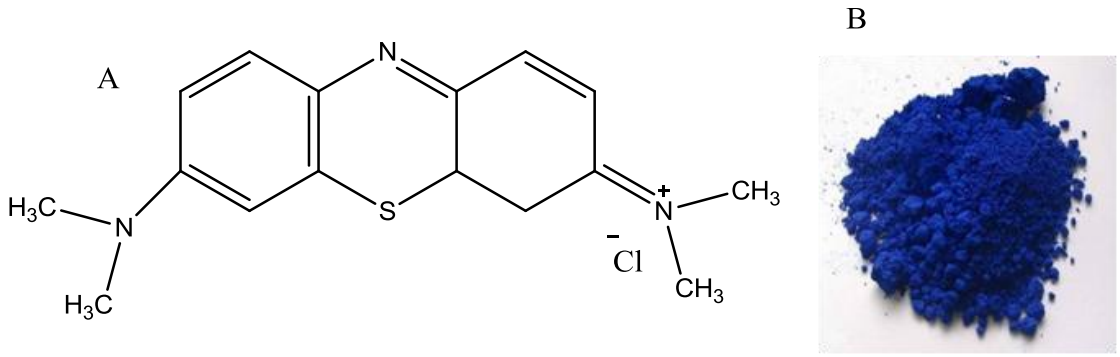

Figure 9. (A) Molecular structure of MB and (B) powder of MB

Despite the importance uses of MB have harmful effects on humans and the environment because of its water solubility. It is noxious, a mutagenic reagent and is supposed to be a cancer-causing dye. Furthermore, MB is possibly harmful to human health and contributes to causing chronic toxicity (Kara *et al*., 2021).

In order to reduce the negative effects of dye contaminated wastewater on humans and the environment, the wastewater must be treated carefully before discharge into main streams. Advances in science and technology have led to the evolution of several techniques for the removal of dyes from industrial (Ahmad *et al*., 2015).

A number of wastewater treatment technologies were investigated for the removal of MB dyes, such as adsorption, ion exchange, electrochemical, oxidation reduction, and catalytic processes. Among the dye removal technologies, adsorption and photocatalysis appears the most economical method because of its inexpensiveness, easy working principle, and high pollutant uptake capacities or degradation but somehow adsorption may cause secondary disposal. (Ahmad *et al*., 2015; Yang *et al.*, 2016).

2.7.1 .Removal of Methylene Blue Using Adsorbent

Despite the development of various technologies for dye waste water treatment, economic, effectiveness and rapid water treatment at a commercial level is still a challenging problem. previous research efforts have focused on the adsorption technology for the dye remediation from wastewater (Begum *et al.*, 2019). This technique can handle fairly large flow rates,

producing a high quality effluent that does not result in the formation of harmful substances, such as ozone and free radicals. Moreover, it can remove or minimize different types of organic and inorganic pollutants and thus has a wider applicability in pollution control. Adsorption is hence recognized as the most versatile process used in lesser developing countries and is currently being used extensively for the removal of organic pollutants from the aqueous media (Mohammed *et al*., 2014).

2.7.2. Photocatalaytical Removal of Methylene Blue

Photocatalysis is a method that involves breaking down or decomposition of varied dyes, organic dirt, and biological species such as harmful fungi and viruses on surfaces with using UV or light irradiation to make it clean (Gangadhar *et a*l., 2021). The process of photocatalytic degradation as one of the potential applications for removing dyes and converting the huge organic compounds to small molecules (Yasin *et a*l., 2021). In case of using the bulk material, the reduction of MB is a kinetically slow process. In case of bulk catalysts, the molecules of MB cannot be adsorbed on the bulk material fast enough.

The existing photocatalysis systems have many shortcomings such as use of expensive light sources and complex/harmful synthesis processes that may obstruct their demand in real world consequently. Apart from acquiring high reduction rates and the complete reduction of the pollutants, the byproducts obtained using this reductive approach are also generally used as synthetic raw materials in various industries as well. Because of these particular reasons, the effort devoted to nanomaterials based catalytic reduction of methylene blue (Begum *et al*., 2019).

2.8. Pathogenic Bacteria Associated with Industrial Wastewater

Industrial waste from food production, particularly from animal processing and leather industries can also be a source of pathogenic microorganisms. The wastewater environment is an ideal medium for both pathogenic and nonpathogenic microorganisms, dangerous pathogens include enteric bacteria, viruses, protozoa, parasitic worms, and their eggs (Chahal *et a*l., 2016).Water borne pathogenic bacteria include *E.coli, Salmonella spp, Staphylococcus aureus, Streptococcus pyogenes*, and *Vibrio spp* contamination in water resources cause diseases (i.e., diarrhea, gastrointestinal illness) (Ojha, 2020). Biological contamination of

water needs to be removed like other pollutant. Traditional antibiotics, which may be either derived from natural products or chemically synthesized, selectively inhibit or kill microbial cells by arresting cellular processes (Xin *et al*., 2019). However, over the years, pathogenic bacteria have developed resistance to traditional methods. Currently, combining two or more active antibiotics is the commonly applied solution to overcome antibiotic resistance with regard to nanomaterials, metal-oxide nanocomposites with distinct morphologies have drawn attention as they combine the properties of the constituent elements to exert a more pronounced and synergistic effect (Jana *et al.*, 2016).

CHAPTER THREE

3. Materials and Methods

3.1. Chemicals

In this study silver nitrate ($AgNO_3$) (Showa, Japan, 98%) was used as a precursor to synthesize silver nanoparticles. Co., Ltd. Japan. Iron chloride tetrahydrate ($FeCl_2.4H_2O$ 98%) and iron (III) chloride anhydrous ($FeCl_{3)}$ 98%) (UN-CHEM CHEMICAL REAGENT as the precursor of iron oxide nanoparticles, sodium hydroxide (China CENTRAL DRUG HOUSE(P) LTD NaOH 97%) was used to adjust pH and for completion of the reaction and to adjust the pH of MB solution. Hydrochloric acid (HCl 36-38%, Sigma-Aldrich, India) was used to adjust the pH of MB solution. Urea was used for the synthesis of graphitic carbon nitride (India, Sigma Aldrich). Methylene blue (98% India, Sigma Aldrich) was used as a representative dye.

3.2. Instrument Used for Characterization

The oven was used to dry synthesized materials while the muffle was furnace used for calcination of urea. UV-Vis Spectroscopy (UV-Vis DRS, Elico SL-150 spectrophotometer Japan) was to obtain absorbance spectra of nanomaterials and in measuring the absorbance of MB dye in the photocatalytic application. X-ray diffractometer (XRD-7000S South Korea) was used to determine the crystalline nature and crystalline size of nanoparticles while Fourier Transfer Infrared Spectroscopy (model FT/IR6600, JAPAN) was used to determine the functional groups in materials. Scanning Electron Microscopy (JCM-6000PLUS Bench Top SEM, JEOL, Japan) was used to determine the morphology of the samples.

3.3. Methods

3.3.1. Collection and Preparation of *Cymbopogan Ctratus* Leaves Extract

A total 2 Kg of *Cymbopogan citratus* was bought from a market of Adama city, East Shoa Zone, Oromia Regional State, Ethiopia. The impurity of *Cymbopogan citratus* leaves was removed by repeated washing with tap water and finally with distilled water. The leaves were dried at room temperature for one week then grinded with an electric grinder and the powder of the leaves was stored for further use.

The aqueous extract of *Cymbopogan citratus* was prepared by heating mixture of 5 grams of *Cymbopogan citratus* powder with 150 ml of distilled water for 2 hours at 40^{o}C by using hotplate while stirring occasionally then cooled, filtered using the Whatman filter paper, and centrifuged. Freshly prepared aqueous extracts was used to synthesize each nanomaterial.

3.3.2. Synthesis of Silver Nanoparticle Using the Extract.

Silver nanoparticles were synthesized according to (Basera *et al*., 2019) protocol with some modification. Previously prepared 5 ml of the plant leaf extract was added to the prepared solution of 5 mM $AgNO_3$ in 50 ml for reduction of silver nitrate into Ag NPs. After 30 minute of stirring by using hotplate, an aqueous solution of 1.0M NaOH was added to the reaction mixture dropwise into the mixture to adjust pH to 11 under stirring and the reaction mixture was refluxed for 1 hour under constant magnetic stirring at 60^{o}C. The prepared Ag NPs were separated with centrifugation at around 3000 RPM and then decantation and washed with deionized water three times to remove any un-reacted plant extract. The prepared Ag NPs were dried in a drying oven at 105^{o}C for 24 hours and stored for further analysis.

3.3.3. Synthesis of Magnetite Nanoparticle Using Extract

The Fe_3O_4 NPs was synthesized following the procedure in the literature with some modification (Yew *et al*., 2016). The prepared solution of Fe^{3+} and Fe^{2+} with 2:1 M ratio respectively was mixed with 5 ml of extract to obtain a yellowish colloidal solution. Then, the pH of the solution was adjusted to 11 by freshly prepared 1.0 M of NaOH adding dropwise to the solution under continuous stirring. The solution refluxed for one hour with continuous stirring at 60^{o}C then Fe_3O_4 NPs were separated using a permanent magnet and washed several times using deionized water. The separated Fe_3O_4 NPs were dried in an oven at around 105°C for 24 hours. The dried sample stored in an airtight container for further analysis

3.3.4. Preparation of Graphitic Carbon Nitride

g-C_3N_4 was prepared from urea as described in the previous literature with some modification (Thurston *et al*., 2017) . Briefly, 50 grams of urea was placed into a ceramic crucible with cover and heated at 550^{o}C for 4 hours in a muffle furnace. The yellowish material was collected, cooled naturally to room temperature, and grounded into the powdered form for further use.

3.3.5. Synthesis of Ag-Fe_3O_4 Nanocomposites

To synthesis Ag-Fe_3O_4 NC (Venkateswarlu *et al*., 2015) protocol was used to prepare Ag-Fe_3O_4 NC. Ag-Fe_3O_4 NC was prepared by mixing 2 grams of the previously synthesized Fe_3O_4 nanoparticle and 100ml of extract in a 250 ml round bottom flask, 5 ml of 5 mM silver nitrate solution was added and stirred for 15 minutes. NaOH solution was added to the reaction mixture to obtain pH 11 and the reaction mixture was refluxed for 1 hour at 60^oC under constant magnetic stirring. A black color precipitate was indicating the formation of Ag-Fe_3O_4 nanocomposites. The black precipitate was separated by applying an external magnetic field and washed with distilled water then stored for further analysis.

3.3.6. Preparation of Ag-Fe_3O_4/g-C_3N_4 Nanocomposites

The Ag-Fe_3O_4/g-C_3N_4 nanocomposites was prepared according to (Yang et *al*., 2016) with minor modifications. Ag-Fe_3O_4 nanocomposites were prepared by mixing 1 gram of the previously synthesized Fe_3O4 nanoparticle and 100 ml extract in a 250 ml round bottom flask, 5 ml of 5 mM silver nitrate solution was added and stirred for 15 minutes. NaOH solution was added to the reaction mixture to obtain pH 11 and the reaction mixture was refluxed for 1 hour at 60^oC under constant magnetic stirring. 2 grams of previously prepared g-C_3N_4 was mixed with 10 ml of distilled water and sonicated in ultrasonication for 3 hours. After the solution of Ag-Fe_3O_4 NC cooled down at room temperature, was mixed with g-C_3N_4 suspension and stirred for one hour at 80^oC. The resulting Ag-Fe_3O_4/g-C_3N_4 nanocomposites separated from the solution with an external magnet and were washed several times with water. Finally, the nanocomposites were dried at 60°C in the oven and ready for further use.

3.3.7. Photocatalytic Activity

Photocatalytic degradation of methylene blue was carried out by using green synthesized AgNPs, Ag-Fe_3O_4 NC, and Ag-Fe_3O_4/g-C_3N_4 NC under visible light irradiation by using optimized condition. 20 mg of biosynthesized nanocomposites was added to 100 ml of 20 ppm methylene blue solution at pH 10 for 60 minutes. The reactions were carried out in a continuous magnetic stirring photoreactor. Before being exposed to irradiation, the reaction suspension was mixed by an ultrasonicated stirrer for 30 minute to obtain the equilibrium state of the working solution. Afterward, the dispersion reactions were carried out in a continuous magnetic stirrer photoreactor with 400 W Osram lamps. The sampling (about 3 ml) was done

every 10 minutes. The samples were separated with an external magnet and the absorbance of MB was determined by UV–Vis spectrometry

The effectiveness of the degradation process calculated from the absorption intensity at 664 nm using the following equation.

Dye degradation (%) = [(Ao - At)/Ao] x 100……...Equation 3

Where Ao is the initial absorbance of dye solution and At is absorbance of the dye solution after t hours of exposure in UV lump irradiation (Yang *et al*., 2016).

The kinetics can be described by a pseudo-first-order equation as suggested by Lagergren (1898) (Aly *et al*, 2018).

$$\log(q_e - q_t) = \log q_e - \frac{k_{p1}}{2.303} \ldots\ldots\ldots\ldots\ldots\ldots\ldots\ldots\ldots\ldots\ldots\ldots\ldots\text{Equation 4}$$

Where q_e and qt (mg/g) are the degradation capacities at equilibrium and time t (min), respectively, K_{p1} (min^{-1}) is the pseudo first order rate constant for the kinetic model

The pseudo-second-order equation developed by Ho and McKay (1999) has a linear form) (Aly *et al*, 2018).

$$\frac{\mathrm{t}}{q_t} = \frac{1}{K_2\ \mathrm{q_e}^2} + \frac{1}{q_e}\mathrm{t} \ldots\ldots\ldots\ldots\ldots\ldots\ldots\ldots\ldots\ldots\ldots\ldots\ldots\ldots\ldots\text{Equation 5}$$

3.3.8. Recyclability of Ag-Fe_3O_4/g-C_3N_4 NC

The recyclability studies were carried out using optimized condition 20 mg of catalyst, 20 ppm of MB solution, and at pH 10 for five successive cycles. The reactions were carried out in a continuous magnetic stirring photoreactor. Before being exposed to irradiation, the reaction suspension was mixed by an ultrasonicated stirrer for 30 minute to obtain the equilibrium state of the working solution. Afterward, the dispersion reactions were carried out in a continuous magnetic stirrer photoreactor with 400 W Osram lamps. The sampling (about 3 ml) was done every 10 minutes. The samples were separated with an external magnet and the absorbance of MB was determined by UV–Vis spectrometry. The catalyst was recovered by using external magnet then washed with distilled water then dried for 2 hours in oven.

3.3.9. Antibacterial Activity

The antibacterial activities of synthesized nanomaterials were done in collaboration with the Department of Applied Biology, Adama Science and Technology University. The antibacterial activities were done against two Gram-negative bacteria species (*E. coli,* and *P. aeruginosa*) and two Gram-positive bacteria (*S. pyogenes* and *S. aureus*) bacteria by using the standard disc diffusion method. On available broth, the medium was used to subculture bacteria and was incubated at 37 ℃ for 24 hours. Fresh overnight cultures were taken and spread on the agar plates to cultivate bacteria. Sterile paper discs of 6 mm diameter saturated with synthesized nanomaterials was used (Geeth *et al.*, 2014).

CHAPTER FOUR

4. Result and Discussion

4.1. Synthesis of Nanomaterials

In this study Ag NPs, Fe_3O_4 NPs, g-C_3N_4, Ag-Fe_3O_4 NC and Ag-Fe_3O_4/g-C_3N_4 NC were synthesized by using *Cymbopogon citratus* leaves as reducing agent. All the nanoparticles and the nanocomposites were prepared under alkaline conditions at room temperature. During Ag NPs synthesis the solution color was changed from pale yellow to ruby red and finally to dark yellowish brown colored solution which indicate reduction of silver ions during the reaction. The dark yellowish-brown color indicates the formation of silver nanoparticles in the reaction mixture (Geetha *et al*., 2014). During Fe_3O_4 NPs preparation the color of the reaction mixture of Fe^{+3} and Fe^{+2} salts and the extract changed from yellow to brown black, after addition of NaOH, which indicates the formation of Fe_3O_4 NPs. The synthesized Fe_3O_4 NPs is able to be attracted by an external magnet which indicates that Fe_3O_4 NPs possessed magnetic properties. The resulting pale yellow solid free flowing powder upon calcinating urea confirmed the formation of g-C_3N_4. Ag-Fe_3O_4 NC and Ag-Fe_3O_4/g-C_3N_4 NC were successfully prepared using aqueous extract of *Cymbopogon citratus* leaves as reducing and capping agent. Both synthesized nanocomposites are able to be attracted by an external magnet which indicates that nanocomposites possessed magnetic properties, so Ag-Fe_3O_4/g-C_3N_4 NC heterostructure photocatalyst with magnetic properties was synthesized by green method.

4.2. Characterization

4.2.1. UV-Vis Spectrophotometer Analysis

The plasmonic absorbance phenomenon of nanoparticles makes it detectable by UV-Vis spectrophotometer (Ijaz *et al*., 2020).

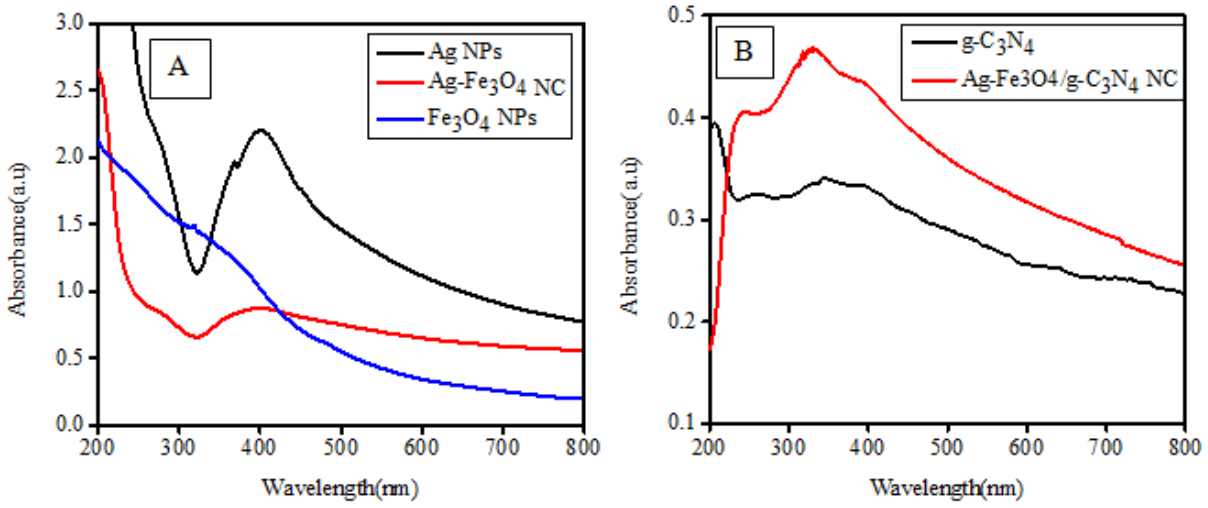

Figure 10. Optical properties analysis (A) Ag NPs, Fe_3O_4 NPs and Ag-Fe_3O_4 NC and (B) g-C_3N_4 and Ag-Fe_3O_4/g-C_3N_4 NC

The synthesized Ag NPs showed a maximum absorption spectrum at around 435 nm (Figure 10A) suggesting the bioreduction of silver nitrate into silver nanoparticles. The maximum absorption spectra of silver nanoparticles formed in the reaction mixture has increasingly sharp absorbance maximum peak 435 nm which was due to the availability of more reducing biomolecules for the reduction of silver ions and this absorption band is in the range of other reports(Ajayi & Afolayan, 2017; Padmavathy *et al*, 2017; Vanlalveni *et al*., 2021). The synthesized Fe_3O_4 NPs (Figure 10A blue line) revealed absorption peak at 250 nm. The formation of Ag-Fe_3O_4 nanocomposite structures display absorption peaks at wavelengths of 430 nm as indicated in Figure 10A (blue line) increased absorbance intensity at 430 nm is an indication of the presence of silver content in the nanocomposites.

Figure 10B (black line) indicated the UV-visible absorption spectrum of prepared g-C_3N_4 shows, sharp absorption peak at 250 nm attributed to the aromatic ring's (π to π^*) transition and absorption peak at 350 nm is due to (n to π^*) transitions caused by electron transfer from nitrogen non-bonding orbital to aromatic anti-bonding which is in agreement with research work of Kumar and co-author (Kumar & Kumar, 2016). After the decoration of Ag-Fe_3O_4 NC with g-C_3N_4 as showed in Figure 10B (red line) the absorbance intensity was dreaded and a broad absorbance spectrum was observed. Increase absorbance may lead to high photocatalytic activity (Huang *et al*., 2012).

The conduction band energy E_{cb} (eV) was calculated directly from the UV-visible absorption spectra by using the following Einstein's photon energy equation (Gharibshahi *et al*., 2017).

$$Ecb = \frac{hc}{\lambda max} \quad \text{.....Equation 6}$$

Were λmax is the maximum absorbance wavelength, h is the Planck constant and c is the speed of light. The calculated conduction band energy 2.3, 2.1, 2.5, 2.7.1, 3.04 eV, for Ag NPs, Fe_3O_4 NPs, Ag-Fe_3O_4 NC, g-C_3N_4 and Ag-Fe_3O_4/g-C_3N_4 NC respectively

4.2.2. FTIR Spectrophotometric Analysis

The prepared nanoparticles and nanocomposites were subjected to FTIR spectroscopy measurements. It was recorded by using a spectrometer in the range 4000-500 cm^{-1}. It was used to identify the possible biomolecules/functional groups adhered to the surface of the nanoparticles and which might have acted as capping agents of the nanoparticles and the functional group of nanocomposites (Viju & Prem, 2018).

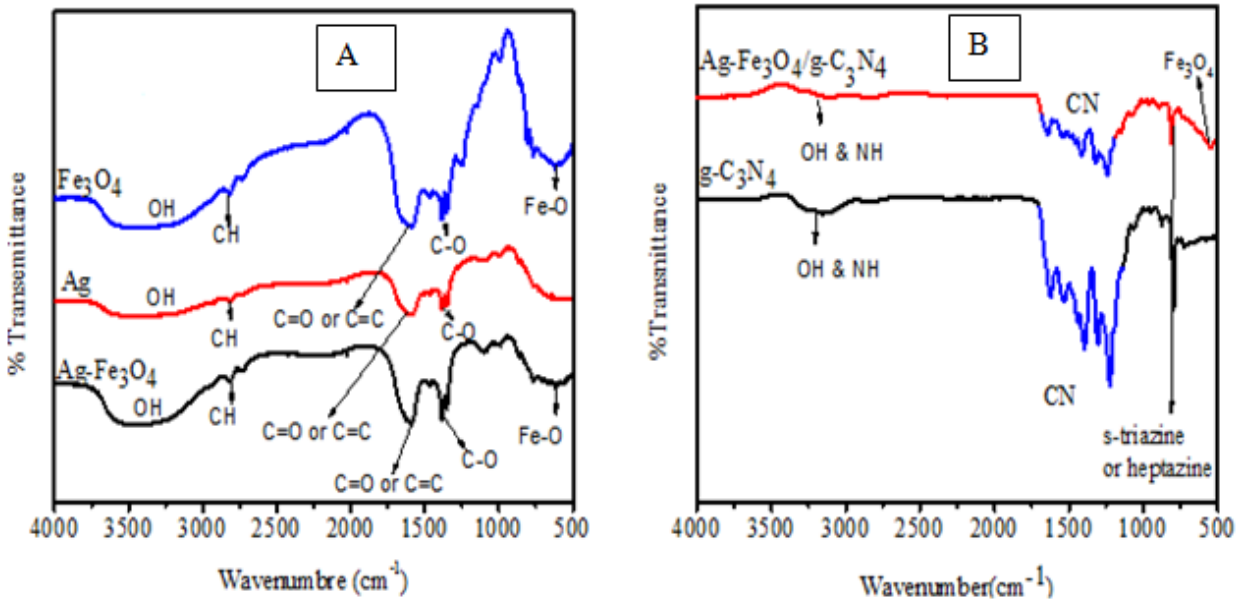

Figure 11. FTIR spectra of (A) Ag NPs, Fe_3O_4 NPS, and Ag-Fe_3O_4 NC, and (B) FTIR spectra of g-C_3N_4 and Ag-Fe_3O_4/g-C_3N_4 NC

It is evidenced from the FTIR results Figure 11A that there are different functional groups on the surface of synthesized Ag NPs, Fe_3O_4 NPs and Ag-Fe_3O_4 NC which indicate the incorporation of biomolecules in with nanomaterials. The broad FTIR absorption band centered at 3500 cm^{-1} indicated the presence of hydroxyl functional group (OH) on the surface of nanoparticles (Baganizi *et al*., 2017). Broad absorption band centered at 2800 cm^{-1} may be sp^3 C-H stretch of biomolecules on the surface of nanomaterials (Dutta, 2017).

The stretching vibration of the carboxylate group C=O FTIR absorption spectrum band at 1640-1820 cm^{-1} indicates the presence of ester, ether, carbonyl, or aromatic functional group on the surface of nanomaterials. These groups are mainly derived from heterocyclic compounds of *Cymbopogon citratus* leaves extract. So it can be assumed that these different water-soluble heterocyclic compounding to such as alkaloids, flavonoids, etc., worked as the capping agent for the synthesis of silver and magnetite nanoparticles (Geetha *et al*., 2014). At 550 cm^{-1} small sharp peak appears which confirms the presence of Fe_3O_4 NPs. Characteristic peaks as the peaks lying in the region between 400 and 600 cm^{-1} were corresponding to Fe_3O_4 (Viju & Prem, 2018).

As illustrated in Figure 11B FTIR spectra of g-C_3N_4, Ag-Fe_3O_4/g-C_3N_4 NC, and g-C_3N_4 FTIR absorption band at 3439 cm^{-1} is due to N-H stretching (Dutta, 2017) and the peaks at 1602 cm^{-1}, 1363cm^{-1}, 1236 cm^{-1}, correspond to the typical stretching modes of the CN heterocycles. The sharp peak around 800 cm^{-1} is due to s-triazine or from heptazine ring units, and when to result of another study excellent agreement with (Thurston et al., 2017). While many peaks located between 750 cm^{-1} and 1750 cm^{-1} are generally related to g-C_3N_4. For the magnetite, there is a sharp peak observed around 550 cm^{-1}.

4.2.3. XRD Analysis

The crystalline structure of the synthesized nanoparticles and nanocomposites was investigated by the X-ray diffraction using X-ray diffractometer. XRD spectrum was recorded from 10^o to 80^o with 2θ angles using CuKα λ=1.54056 Aº radiation operated at 40 kV and 30 mA. Debye Scherer's equation indicated in equation 2 was used to estimate the average crystallite size of the synthesized nanoparticles.

. The lattice parameter nanoparticles from XRD result is determined by (Chaki *et al*., 2015).

$$d_{hkl} = \frac{a}{\sqrt{h^2+k^2+l^2}}$$ ……..Equation 7

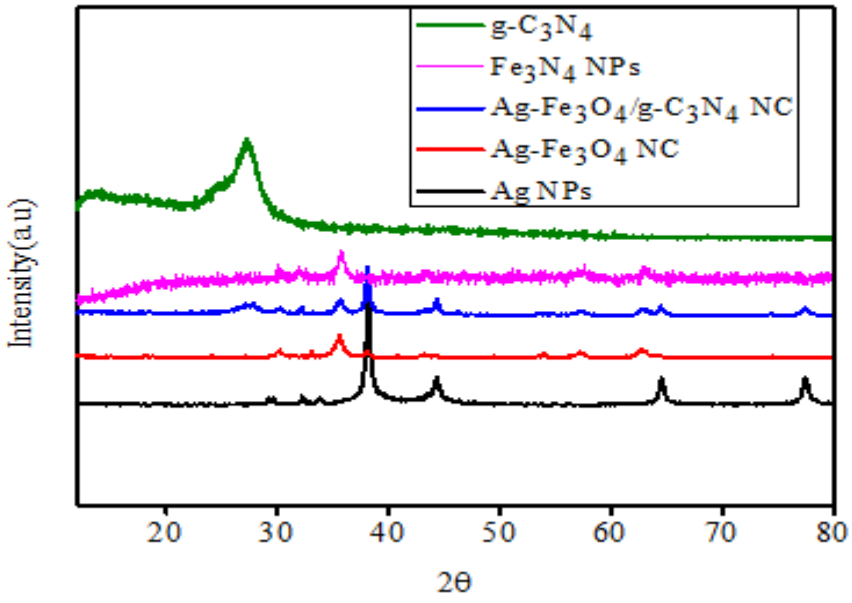

Figure 12. XRD patterns of Fe_3O_4 NPs, Ag NPs, Ag-Fe_3O_4 NC, g-C_3N_4, and Ag-Fe_3O_4/g-C_3N_4 NC

The solid-state structure of synthesized g-C_3N_4 was investigated by X-ray diffraction as shown in Figure 12. The powder X-ray diffraction pattern showed the successful formation of the desired graphitic phase indicating, (002) reflection located at 2θ = 27.2° (d = 3.25 Å), and there is a small reflection peak located at 2θ =13°, it suggests an in-plane structural packing motif of g-C_3N_4 gives information about interspacing among nitride pores (Thurston *et al*., 2017). The (100) reflection is observed at 2θ = 13° was closely related to the dimensions expected from the individual melon subunits (d = 6.8 Å), and these two diffraction peaks are consistent with the XRD patterns of reported g-C_3N_4 (Zhang *et al*., 2017). So XRD analysis results confirmed the successful formation of g-C_3N_4 from thermal polymerization of urea.

The XRD pattern Fe_3O_4 NPs synthesized using plant extract is shown in Figure 12. Representative diffraction peaks at 2θ = 30.3°, 35.35°, and 63.1° which correspond to the (220), (311), and (440) planes (JCPDS card no. 79-0417), respectively belong to Fe_3O_4 phase (Yew *et al*., 2016). The reflection peak position and relative intensities were well matched with the standard of Fe_3O_4 NPs at 2θ = 35.767° and confirmed the inverse cubic spinal

structure of the synthesized material. The average crystallite size of the synthesized magnetite NPs was calculated by the width of the reflection peak according to the Debye–Scherer's equation and the crystalline size was found to be 10.79 nm.

Table 1: The crystalline size and lattice parameter value of biosynthesized Fe_3O_4 NPs

Peak position(2θ)	FWHM	size of the nanoparticle (nm)	Average size (nm)	d-spacing (nm)	Lattice Parameter, a (Å)	hkl
30.33	0.93872	8.77	10.79	2.9445	8.33	220
35.767	0.81067	10.3		2.5084	8.32	311
63.1	0.66588	13.3		1.4721	8.327	440

Table1 shows a summary of parameters extracted from the XRD spectra of the greenly synthesized Fe_3O_4 nanoparticle. The calculated average size of this particle is small enough and close to super magnetite Fe_3O_4. The XRD pattern of synthesized silver nanoparticles showed several peaks, where the four main and intense peaks located at 38.7°, 44.3°, 64.5°, and 77.54°, corresponding to the (111), (200), (220) and (311) planes, respectively.

Table 2: The crystalline size and lattice parameter value of biosynthesized Ag NPs

Peak position (2θ)	FWHM	size of the nanoparticle (nm)	Average size (nm)	d-spacing (nm)	Lattice parameter(Å)	hkl
38.16	0.4425	18.2	18.67	2.35643	4.0814	111
44.2	0.5571	15.4		2.04251	4.085	200
64.5	0.4543	20.68		1.44304	4.0815	220
77.54	0.4995	20.4		1.23127	4.0836	311

Table 2 indicates that the silver nanoparticles formed by the reduction of Ag^+ ions using *Cymbopogon citratus* extract are crystalline. The peak related to the lattice plane (111) is the most intense suggesting its most predominant orientation in addition to the crystalline nature

of the synthesized silver NPs. Similar results have been reported recently (Jabbar *et al*.,2020). The average crystalline size of silver nanoparticles synthesized using *Cymbopogon citratus* extract was calculated using Scherer's equation and is equal to 18.67 nm. Figure 12 showed the XRD pattern of Ag-Fe_3O_4 NC this results indicated that Ag-Fe_3O_4 NC were successfully synthesized using *Cymbopogon citratus* leaf extract as a reducing agent. The formation of composite photocatalyst Ag-Fe_3O_4/g-C_3N_4 was also confirmed by the XRD pattern of composite each expected peak (Figure 12). The extra peaks was observed on Ag-Fe_3O_4/g-C_3N_4 NC but not observed in Ag-Fe_3O_4 NC at 2θ values of 27.6º corresponding to the crystal planes (002) indicated the presence of g-C_3N_4. Further, we notice that the incorporation with Fe_3O_4 NPs the diffraction peak of g-C_3N_4 at 27.2 is lowered the intensity. Have also reported the same phenomena and they suggested that the lowering of this peak is due to the restraining the stacking of g-C_3N_4 perpendicular to the direction owing to introducing Fe_3O_4 (Pant *et al*., 2017). The XRD analysis suggests Ag and Fe_3O_4 NPs are well attached on the surface of g-C_3N_4 surface and the XRD finding confirmed Ag-Fe_3O_4/g-C_3N_4 nanocomposites well synthesized by using *Cymbopogon citratus* leaves extracts.

Table 3: The crystalline size of Ag and Fe_3O_4 NPs in synthesized nanocomposites

The variation of crystalline size of Ag and Fe_3O_4 NPs in Ag-Fe_3O_4 NC				The variation of crystalline size of Ag and Fe_3O_4 NPs in Ag-Fe_3O_4/ g-C_3N_4 NC			
2theta	FWHM	Crystalline size	Average size (nm)	2theta	FWHM	Crystalline size	Average size (nm)
30.175	0.92813	8.865	12.57	30.27	0.944	8.13	11.37
35.57	0.76704	10.88		35.64	0.895	8.455	
38.1	0.34185	24.6		38.122	0.47	15.97	
43.421	1.53557	5.569		44.3	0.78	9.434	
53.901	0.9179	9.79		57.32	0.62	11.257	
57.23	1.24989	7.24		62.91	0.712	9.53	
62.83	1.40699	6.62		64.482	0.455	14.8	
77.44	0.3754	27.3		77.4351	0.4875	12.72	

The calculated average crystal size of synthesize nanomaterials are given in Table 3 and dcreased in the crystalline size was observed for Ag NPs. In figure 12 the intensity of peak of Ag NPs in composites were decreased due to crystalline domain size decreases further, peak broadening increases and the signal intensity will be decreased (Materials 2019). The crystalline size of Ag NPs decreased from 18.67 to 12.5 nm. The decreased intensity may indicate that insufficient energy to crystallites to orient in proper equilibrium sites and causes and decrease in intensity.

4.2.4. SEM Analysis

The images of the synthesized nanomaterial surface were examined using scanning electron microscopy (SEM) to investigate the shape, size, and porosity of the materials before and after doping and decoration.

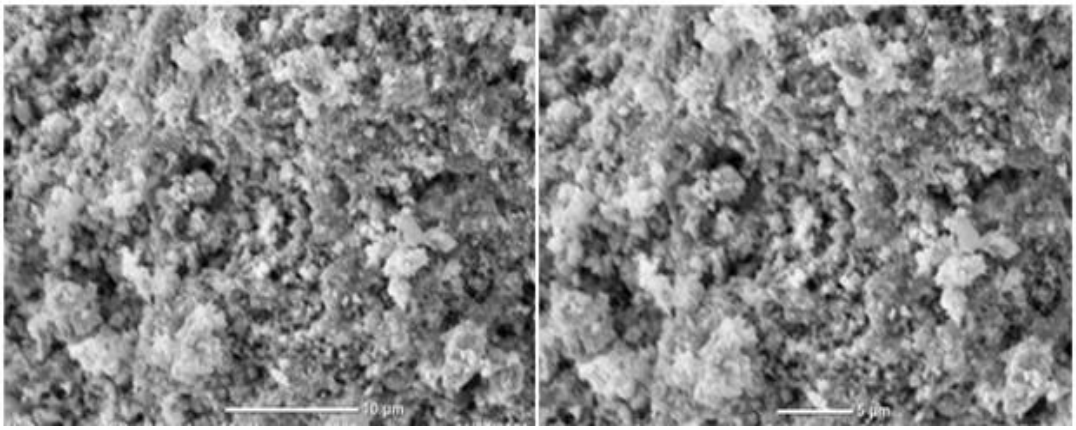

Figure 13. SEM images of Ag NPs

As SEM image in Figure 13 indicate silver nanoparticles synthesized using *Cymbopogon citratus* leaf extract as reducing and capping agent has spherical shape with some aggregation and different size of Ag NPs observed this also confirmed by UV-Vis analysis (Figure 10) reveled peak shift. As well as in the XRD result the calculated crystalline size varied from 15.4-20.68 nm.

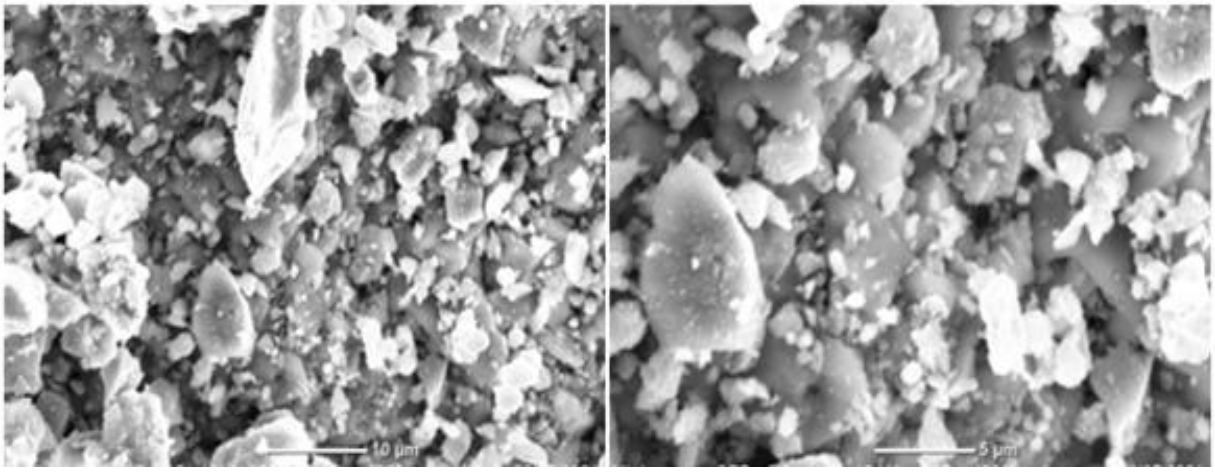

Figure 14. SEM images of Fe_3O_4 NPs

Figure 14 show SEM images of Fe_3O_4 NPs crystallites are nearly square in shape and it can be seen that the particles agglomeration, indicating a good connectivity between the grains together and the size. Additionally some porosity is observed in SEM image of Fe_3O_4 NPs which helps for adsorption proprieties of materials.

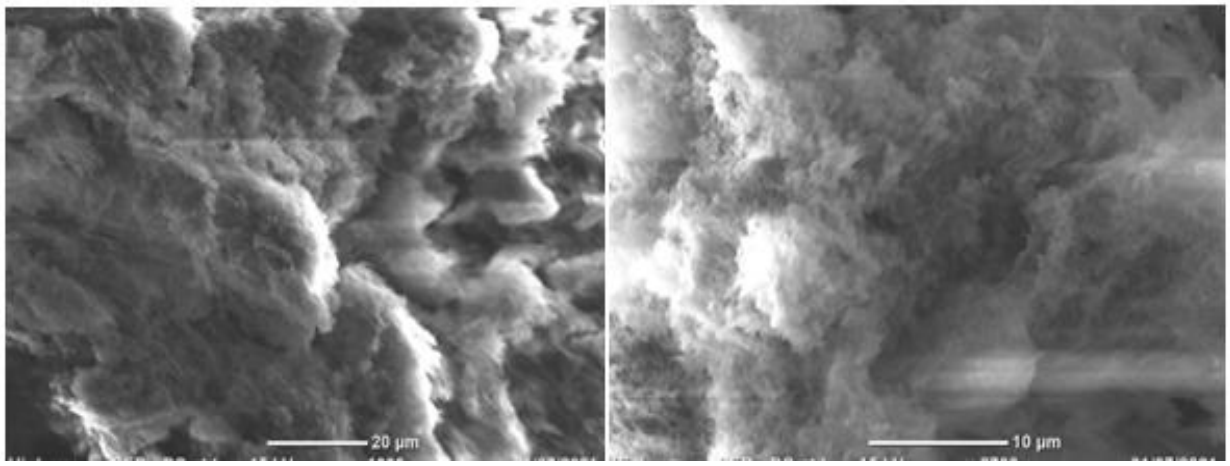

Figure 15. SEM images of g-C_3N_4

As shown in Figure 15 (SEM images of g-C_3N_4)), the synthesized g-C_3N_4 has amorphous sheet like structure rather than particles nature (Liu *et al*., 2020). SEM image shows its sheet structure with visible pores embedded in the nano sheets, in agreement with literature reports and the amorphous structure agrees well with the XRD data.

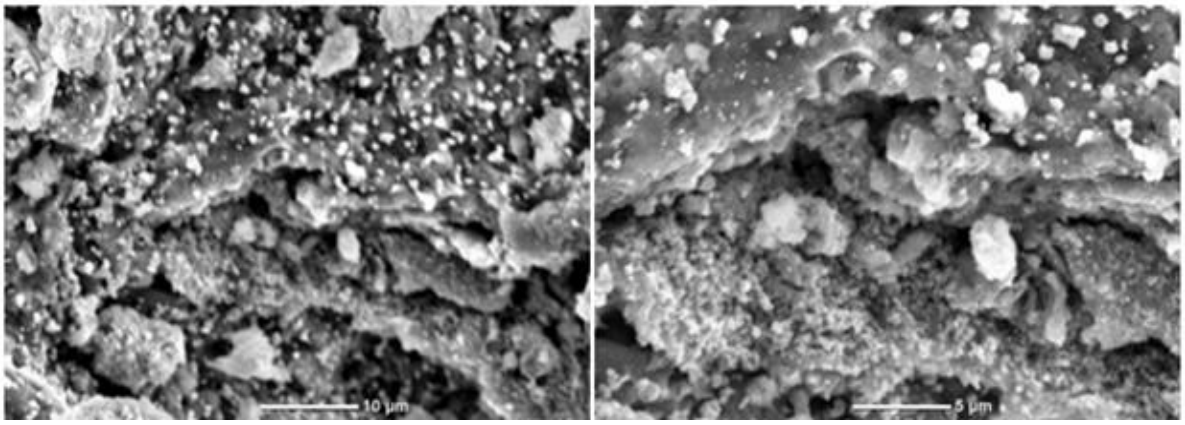

Figure 16. SEM images of Ag-Fe_3O_4 Nanocomposites

SEM image of Ag-Fe_3O_4 NC was shown in Figure 16 and the nanocomposite has spherical nanostructure with some aggregation. As indicated in SEM images, Ag NPs are dispersed on the surface of Fe_3O_4 and combined nanostructure formed in nanocomposite.

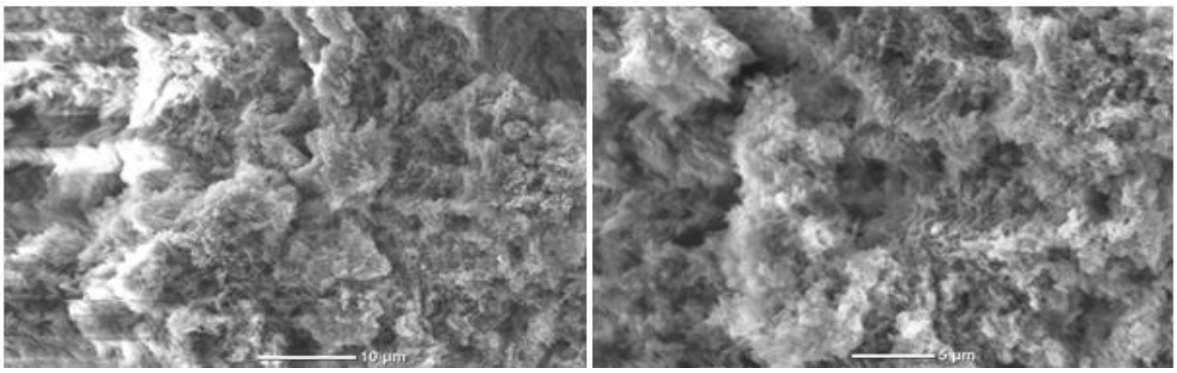

Figure 17. SEM images of Ag-Fe_3O_4/g-C_3N_4 NC at different magnification power

As illustrated in Figure17 the morphology of composite exhibited uniform distribution of Ag-Fe_3O_4 NC throughout the surface of g-C_3N_4 sheets. The Ag-Fe_3O_4 dispersed throughout the solution and decreased the C_3N_4, but high amount g-C_3N_4 sheets were observed. In this case, the large g-C_3N_4 sheets act as an excellent support to stabilize the formation of Ag-Fe_3O_4 nanoparticles.

4.3. Photocatalytic Activity of Synthesized Nanomaterials

The variations in different experimental conditions affecting photocatalysis of methylene blue using photocatalyst Ag-Fe_3O_4/g-C_3N_4 NC, included pH , amount of catalyst, and initial dye

concentration were taken into account to reach an integrated model for the photocatalytic degradation of methylene blue using Ag-Fe_3O_4/g-C_3N_4 NC. The amount of these parameters were selected based on past studies (Aly.*et al*, 2018; Pant *et al*., 2017). Furthermore, the photocatalytic degradation rate is also studied by using the synthesized nanomaterials (Ag NPs, Ag-Fe_3O_4 NC, and Ag-Fe_3O_4/g-C_3N_4 NC) for comparison. Additionally the recyclability Ag-Fe_3O_4/g-C_3N_4 NC was investigated.

4.3.1. Effect of pH

The pH value of dye solution has a significant role in the degradation process, which influences the charge properties of the surface (Tju *et al*., 2017). The photocatalytic degradation of methylene blue using the synthesized Ag-Fe_3O_4/g-C_3N_4 NC were investigated at different pH (4,6,8,10,12,and 14) while other parameters were kept constant, 100 ml of 10 ppm of MB solution by adding 10 mg of catalyst into the solution for 40 minutes of UV-light irradiation (Figure 18A). It was observed that at pH 4–10 degradation MB increased, but after pH 10 the degradation of MB was unchanged. The maximum dye degradation was observed at pH 10 and it is optimum pH for this reaction using Ag-Fe_3O_4/g-C_3N_4 NC, because beyond this value, the degradation efficiency is unchanged. As methylene blue is a cationic dye subsequently when the pH of the solution increased greater molecules of methylene blue dye were adsorbed on the surface of the catalyst. When pH was acidic, the positive charge of the surface opposed the adsorption of cationic species but as the pH goes from acidic to basic, the surface attained the negative charge so this negative surface attracts the cationic dye due to electrostatic attraction between cationic (Ag-Fe_3O_4/g-C_3N_4 NC) and anionic species (Nguyen *et al*., 2016).

4.3.2. Effect of Catalyst Dosage

Since the degradation of dye is dependent on the amount of catalyst, the photocatalytic activity of Ag-Fe_3O_4/g-C_3N_4 NC was evaluated by varying the amount of catalyst from 5 mg, 10 mg, 15 mg, 20 mg, 25 mg, and 30 mg in 100 ml and 10 ppm of dye solution with 40 minutes UV-light irradiant, pH also arranged at 10 which is optimum pH for this degradation reaction. The degradation percent of MB dye was increased with the increase in catalyst concentration up to 20 mg (Figure 18B) and maximum degradation observed at catalyst dose 20 mg. However, a gradual decrease was observed after the further increase in the catalyst dose. This is maybe

due to the agglomeration of particles may take place and the reaction mixture turned turbid (Sahoo *et al*., 2012).

4.3.2. Effect of Initial Concentration of MB Solution

The effect of various dye concentrations was studied by taking different concentrations of dye (30, 25, 20, 15, 10, and 5 ppm) by maintaining the catalyst dose (20 mg), pH (10), and irradiation time (40 minutes) the result plotted in (Figure 18C). The photodegradation efficiency of methylene blue is inversely proportional to its concentration, which means, the lower the dye concentration, the higher efficiency of the dye photodegradation (Mohamed *et al*., 2012). The obtained data shows the degradation decreased with increasing the dye concentration, at low MB concentration significant changes was not observed. But notable change of removal efficiency were observed with further increases in the dye concentration, the reaction mixture having a higher dye concentration than 20 ppm showed a significant decline in degradation efficiency.

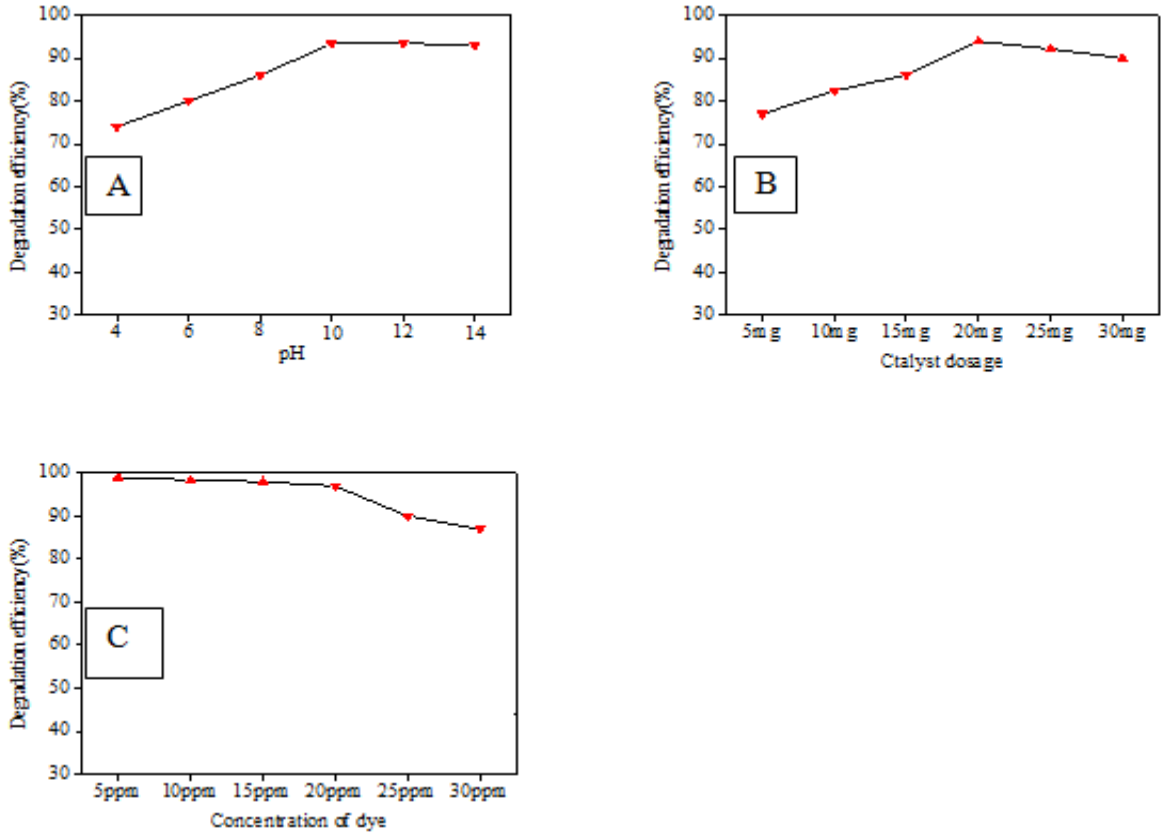

Figure 18. Effect of (A) pH, (B) catalyst dose, and (C) dye concentration against degradation efficiency of Ag-Fe_3O_4/g-C_3N_4 NC.

4.4. Kinetic Study of Synthesized Nanomaterials

The photocatalytic activity of the synthesized Ag NPs, Ag-Fe_3O_4 NC, and Ag-Fe_3O_4/g-C_3N_4 NC for the decomposition of MB dye solution under visible light irradiation, and to compare the photocatalytic activity of each nanomaterial. The photodegradation activities of nanomaterials were evaluated by the degradation of an aqueous solution of a concentration of 100mL of methylene blue (MB solution 20 ppm) by adding 20mg of catalyst. By maintaining the room temperature and pH 10 at a time interval of 10 minutes for 60 minutes of UV light irradiation.

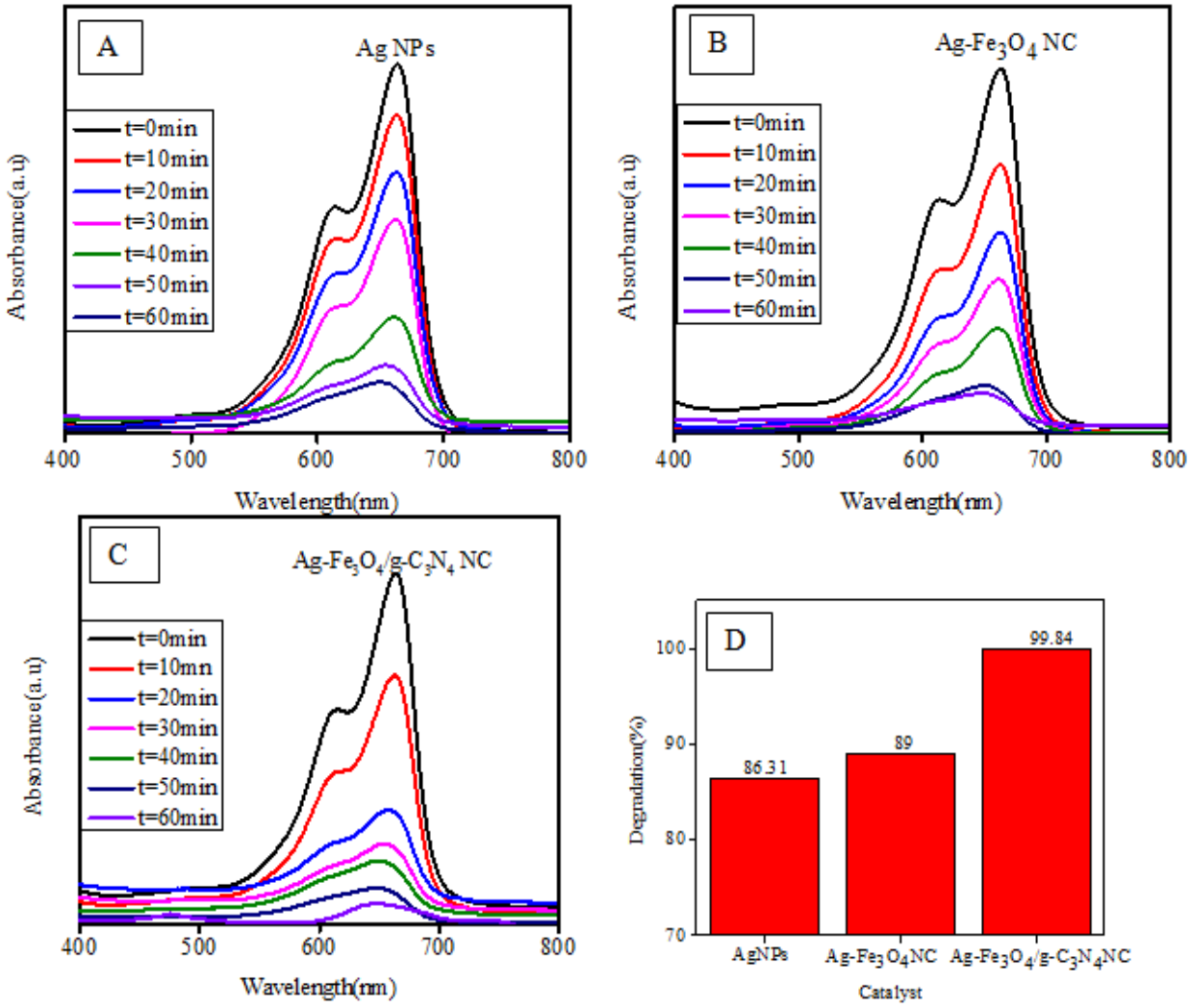

Figure 19.UV-Vis spectra of Methyelen blue degradation by (A) Ag NPs, (B) Ag-Fe_3O_4 NC, (C) Ag-Fe_3O_4/g-C_3N_4 NC and (D) maximum removal efficiency of synthesized nanomaterials.

Pure Ag NPs show decreased peaks for methyelen blue with increasing irradiation time (Figure 19A), however exhibited weak photocatalytic activity that only degraded MB < 86.31% 60 minute of UV light irradiation. Ag-Fe_3O_4 nanocomposite showed somehow enhanced ability to degrade MB compared to pure AgNPs. Percentage degradation efficiency of silver magnetite nanocomposites was calculated as 89% at 60 minutes UV light irradiation. So the combination of Ag NPs with Fe_3O_4 NPs has been used to accelerate the photocatalytic property of Fe_3O_4 NPs because the Ag NPs have shown an enhanced electron hole separation and interfacial charge transfer ability, as well as the increase of visible light excitation of Fe_3O_4NPs (Akhundi *et al*, 2016). But significant improvement showed by Ag-Fe_3O_4/g-C_3N_4 NC, 99.84% degradation efficiency of MB was observed after 60 minute of irradiation. And this study also confirmed g-C_3N_4 can accelerated photocatalytic property of Ag-Fe_3O_4 nanocomposite.

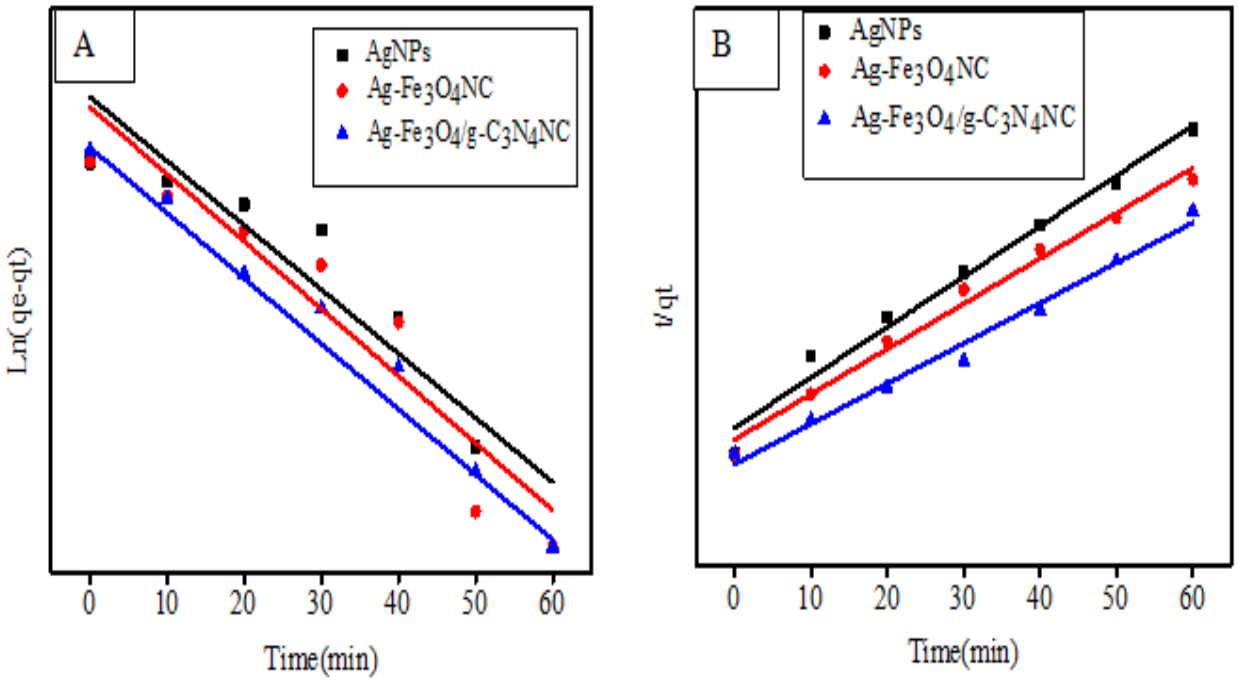

Figure 20. (A) Pseudo-first-order and (B) pseudo-second-order kinetic model for removal of methylene blue

Table 4: Different parameters of the pseudo-first-order and pseudo-second-order kinetic model

Catalyst	Pseudo-first-order kinetics parameter				pseudo-second-order kinetics parameter			
	K1(min^{-1})	R^2	Slope	Intercept	K2(min^{-1})	R^2	Slope	Intercept
AgNPs	0.0776	0.865	4.6515	-0.02491	0.000205	0.991	0.0123	0.1222
Ag-Fe_3O_4NC	0.0778	0.884	4.702	-0.02917	0.00025	0.994	0.0148	0.0833
Ag-Fe_3O_4/g-C_3N_4 NC	0.0072	0.901	4.32	-0.03186	0.000325	0.998	0.0195	0.01605

The photocatalytic degradation of methylene blue cheeked by the pseudo-first and second order kinetic according to the Langmuir-Hinshel- wood model. Figure 20A shows the non linear relationship between Ln(qe-qt) and the reaction time, confirming the degradation of MB solution not fitted with pseudo first-order kinetics. The value of R^2 calculated from the pseudo-second-order model is more closely1; this indicates that the pseudo-second-order model fit. The high photocatalytic rate is obtained for Ag-Fe_3O_4/g-C_3N_4 NC. It can be concluded that pseudo-second-order modal was the best fit for degradation of MB using Ag-Fe_3O_4/g-C_3N_4 NC, the same result were obtained in the previous study (Aly & Abd-elhamid, 2018). Linear regression correlation coefficient (R^2) or high correlation coefficients indicate that experimental data exhibit a good compliance with pseudo-second order kinetic model. The compliance with the pseudo-second-order model suggested that chemical sorption involving valence forces through sharing or exchange of electrons between adsorbent and adsorbate might be significant (Ernawati *et al*., 2021).

4.5. Recyclability of Photocatalyst

One of the most desirable abilities of photocatalysts is their durability and reusability. In practical usage, the photocatalyst should be chemically stable after successive cycles. Hence,

the recyclability of Ag-Fe_3O_4/g-C_3N_4 nanocomposites was evaluated for MB photodegradation five sequential cycles.

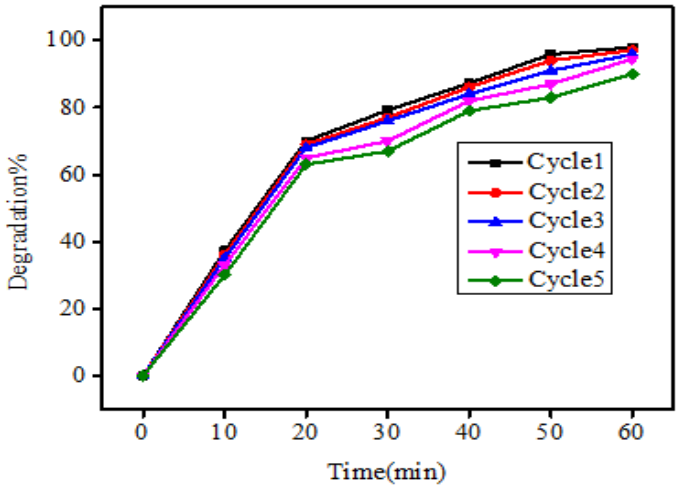

Figure 21. The recyclability of Ag-Fe_3O_4/g-C_3N_4 NC to degrade MB

As presented in Figure 21 slight decrease of the Photocatalytic activity of Ag-Fe_3O_4/g-C_3N_4 nanocomposite was observed after five cycles, which could be due to occupy active sites of nanocomposites by dye molecules during reusability process. When compared to the first cycle only 9.8% the degradation efficiency loss was observed after five successive cycles from 99.84%- 90% decreased. The removal efficiencies of cycles 1, 2, 3 and 4 were found 98- 94% small amount of efficiency loss were observed but in cycle five the degradation efficiency became 90%. This revealed the magnetite NPs are effectively used to easy recovery and handling catalytic activity of Ag /g-C_3N_4 NC for various applications.

4.7. Antibacterial Studies

In this study, *Cymbopogon citratus* leaves extract mediated synthesized Ag NPs, Fe_3O_4 NPs, Ag-Fe_3O_4 NC and Ag-Fe_3O_4/g-C_3N_4 NC at concentrations of 100 µg/ml, 150 µg/ml, and 200 µg/ml were tested for antibacterial activity using gram-negative and gram-positive bacteria strains of *Escherichia coli*, *Pseudomonas aeruginosa*, and *Staphylococcus aureus Streptococcus pyogenes* using disc diffusion method and as a positive control Ciprofloxacin was used. The disk diffusion method was performed as the antibacterial assay.

The pure cultures of all the tested pathogens were inoculated to fresh nutrient broth in separate tubes. The tubes were incubated at 37°C for 24 hours. After 24 hours, turbidity was adjusted to 1×10^5 CFU/ml at a wavelength of 600 nm using a spectrophotometer. The surface of the agar plates was then fully swabbed with different bacterial strains completely ensuring that all the plates receive enough bacterial colonies. The cellulose paper discs were placed in their respective positions on the plates using sterile forceps. The plates were incubated overnight at 37°C. The zones of inhibition were then observed and measured on the next day using a ruler.

Table 5: Antibacterial activity of green synthesized Ag NPs

Bacteria	Zone of Inhibition in (mm)			
	100 µg/ml	150 µg/ml	200 µg/ml	+ve control
E. coli	13	15	20	22
P. aeruginosa	7	10	16	20
S. aureus	10	12	15	18
S. pyogenes	15	12	15	16

Figure 22. Picture of antibacterial activity of Ag NPs

Ps. A were P. *aeruginosa, S.A were S. aureus* and S.P were *S. pyogenes.*

The above table (Table5) shows the antibacterial activity of Ag NPs. The measured zones of inhibitions from Figure 22, high inhibition zone observed for all the four strains, and maximum inhibition zones was 20 mm and 16 mm for *Escherichia coli and Pseudomonas aeruginosa* strains respectively at higher Ag NPs concentrations 200 μg/ml. Even if the cell wall of gram-negative bacteria is narrower than that of gram-positive strains but more susceptible to silver nanoparticles (Yin *et al*., 2020). This reveals the synthesized Ag NPs are small enough for cellular wall penetration. For gram-positive bacteria zone of inhibition was recorded 15 mm for both *Staphylococcus aureus and Streptococcus pyogenes* strains at maximum Ag NPs concentrations 200 μg/ml.

Generally, the antibacterial assay using *Cymbopogon citratus* leaves extract mediated synthesized AgNPs effectively inhibits the growth of both gram-positive and gram-negative bacteria. But for gram-negative is slightly active due to the Ag+ ion electrostatic attraction toward the negatively charged cell membrane of bacteria. This study observed almost the same result, the investigation made by (Geetha *et al.*, 2014). Only the variation seen, at 100 μg/ml concentration showed 13 mm for *Escherichia coli*, for *Pseudomonas aeruginosa* 15 mm, but in our study, only 7 mm zone of inhibition was recorded.

Table 6: Antibacterial activity of green synthesized Fe_3O_4 NPs

Bacteria	Zone of Inhibition in (mm)			
	100 μg/ml	150 μg/ml	200 μg/ml	+ve control
E. coli	8	8	10	20
P. aeruginosa	7	9	10	20
S.aureus	8	8	9	22
S. pyogenes	7	8	8	20

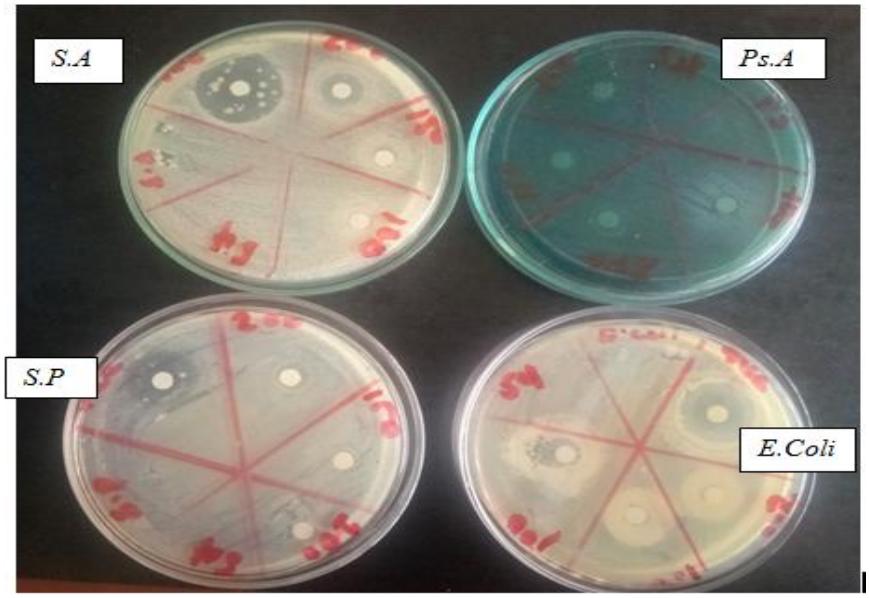

Figure 23. Picture of antibacterial activity of Fe_3O_4 NPs

As Table 6 and Figure 23 shows the synthesized Fe_3O_4 NPs the biggest zones of growth inhibition10mm for both *Escherichia coli and Pseudomonas aeruginosa* and *Staphylococcus aureus and Streptococcus pyogenes* respectively 9 and 8 mm respectively at maximum Fe_3O_4 concentration 200 µg/ml. This difference can be attributed to differences in cell wall structure inherent in gram-negative and gram-positive bacteria. The reason for the bactericidal activity is due to the Fe_3O_4 presence of reactive oxygen species(Sathishkumar *et al*., 2018) .

Table 7: Antibacterial activity of green synthesized Ag- Fe_3O_4 NC

Bacteria	Zone of Inhibition in (mm)			
	100 µg/ml	150 µg/ml	200 µg/ml	+ve control
E. coli	12	14	17	25
P. aeruginosa	13	15	17	20
S. aureus	12	12	16	20
S. pyogenes	10	15	16	20

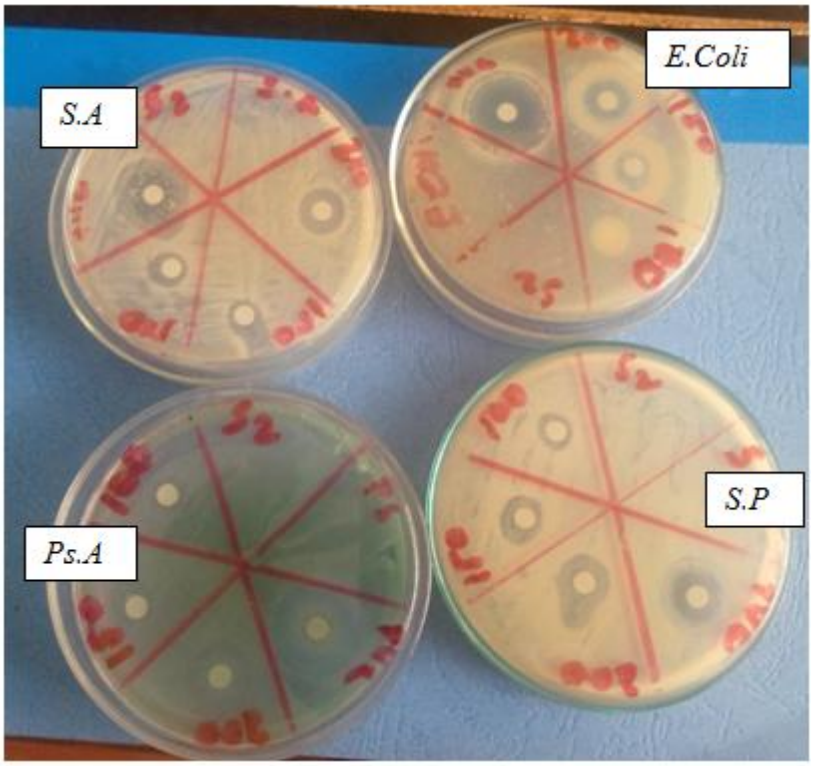

Figure 24. Image of antibacterial activity of Ag-Fe_3O_4 NC

The antibacterial result shown in Table 7 (Figure 24) the Ag-Fe_3O_4 NC reveal that silver nanoparticles incorporated into magnetic nanocomposites have the enhanced antibacterial properties of magnetite nanoparticles.

Table 8: Antibacterial activity of green synthesized Ag-Fe_3O_4/g-C_3N_4 NC

Bacteria	Zone of Inhibition in (mm)			
	100 µg/ml	150 µg/ml	200 µg/ml	+ve control
E. coli	12	14	21	25
P. aeruginosa	13	15	22	24
S. aureus	13	14	17	18
S. pyogenes	14	15	18	20

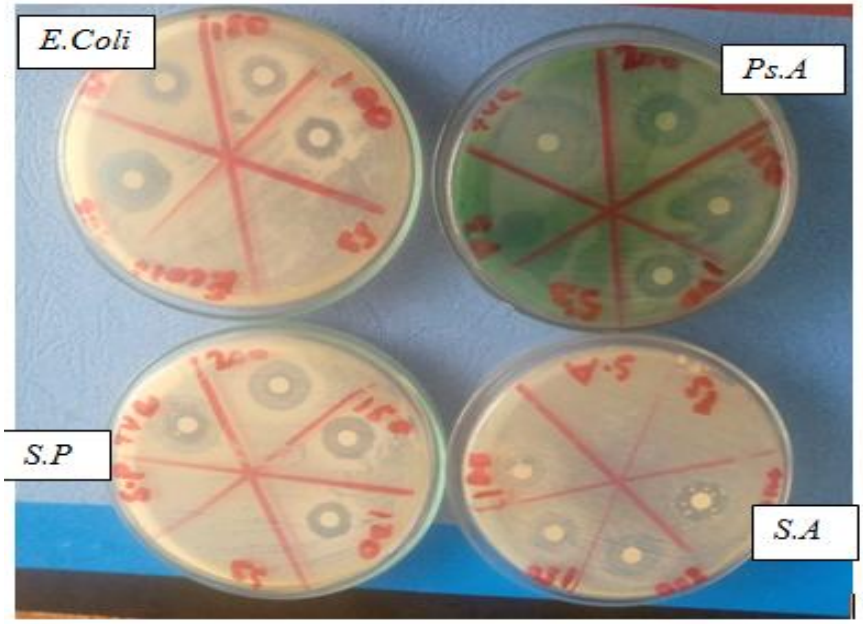

Figure 25. Image of antibacterial activity of Ag-Fe_3O_4/g-C_3N_4 NC

As the past studies reported g-C_3N_4 did not show significant antibacterial activity (Pant, *et al*., 2017) but the recent year research progress reported its antibacterial application, their sharp edges can physically cut bacteria directly like a knife, causing cellular dysfunction and leakage of cytoplasm components through the destruction of bacterial cell walls and membranes (Kong *et al*., 2021).

Also as the Table 8 show the present study confirms synthesized Ag-Fe_3O_4/g-C_3N_4 NC a strong antibacterial performance was observed. Ag-Fe_3O_4/g-C_3N_4 NC (Table 8) shows high zone of inhibition for all bacterial strain, and as concentration increase increased inhibitions was observed.

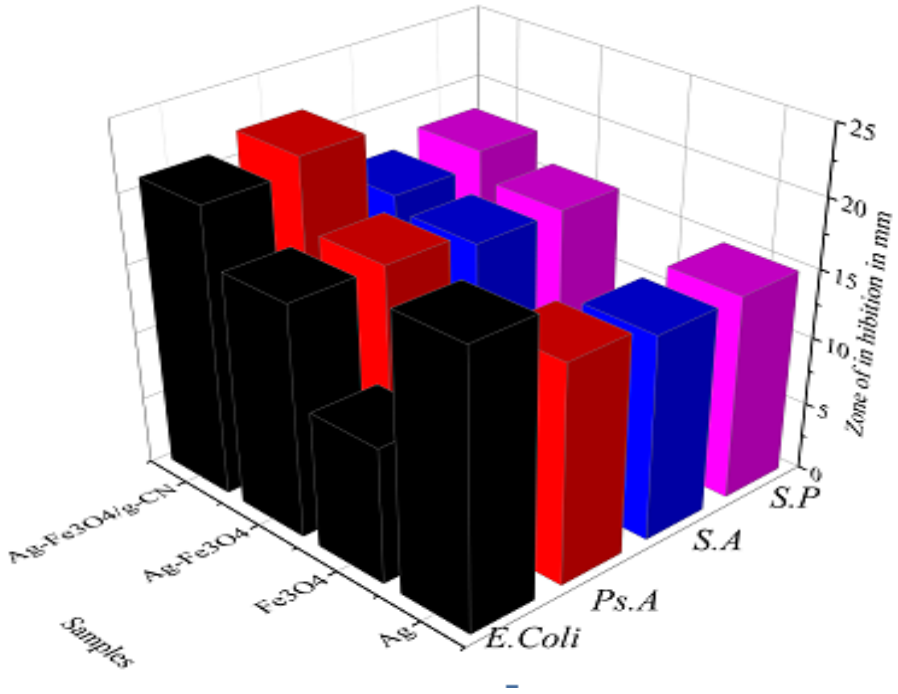

Figure 26. Comparison chart for the antibacterial activity of the synthesized nanomaterials at 200μg/ml concentration.

The above chart shows a comparison of the antibacterial activity between the synthesized nanomaterials at 200 μg/ml concentration. As the above chart reveals pure Ag nanoparticles show high zone of inhibition than Fe_3O_4 nanoparticles because Ag NPs continually release silver ions, which may be considered the inhibitory effect of is attributed to the uncontrolled generation of free radicals from the surface of Ag NPs which attacks the membrane lipids of the microbe leading to the breakdown of membrane function (Pattabi & Pattabi, 2013). An excellent zone of inhibition was obtained against *E. coli* which is 20 mm. Similarly, good antibacterial results were obtained for the composite material. But Fe_3O_4 NPs show less effect in both bacterial strains when compared to the other nanomaterials. So the addition of Ag to Fe_3O_4 NPs enhances the antibacterial activity and also the Ag-Fe_3O_4 NC somehow increased zone of inhibition was observed, 17 mm for gram-negatives and 16 mm for gram-positives. For Ag-Fe_3O_4/g-C_3N_4 NC high and enhanced antibacterial activity was observed in all bacterial strains. 21 mm, 22 mm, 17 mm, 18 mm zone of inhibition recorded for *Escherichia coli*, *Pseudomonas*, *Staphylococcus aureus*, and *Streptococcus pyogenes* respectively. So the present study confirms the synthesized Ag-Fe_3O_4/g-C_3N_4 NC has a strong antibacterial performance.

5. Conclusion and Recommendation

5.1. Conclusion

The present study successfully reports the use of Ag-Fe_3O_4/g-C_3N_4 nanocomposites, which were prepared by green methods to investigate the photocatalytic and antibacterial properties. The calculated average crystal size of synthesize nanomaterials is 11.37 which is small enough and large surface area. Furthermore, parameters such as the effect of pH of the dye solution, catalyst dose, dye concentration and recyclability of Ag-Fe_3O_4/g-C_3N_4 NC were also studied. Ag-Fe_3O_4/g-C_3N_4 nanocomposites demonstrate enhanced photocatalytic effects for the degradation of methylene blue and it is found that pH of the dye solution, initial concentration of dye solution and catalyst are limiting factors photocatalysis degradation. Photodegradation study of MB dye solution was done using Ag NPs, Ag-Fe_3O_4 NC and Ag-Fe_3O_4/g-C_3N_4 NC maximum removal efficiency of 86.31%, 89% and 99.84 respectively were obtained for Ag NPs, Ag-Fe_3O_4 NC and Ag-Fe_3O_4/g-C_3N_4 NC. The antibacterial study of Ag-Fe_3O_4/g-C_3N_4 NC, the measured zone of inhibition was 21 mm for E. coli, 22 mm for P. Aeruginosa, 17 mm for S. Aureus and 18 mm for S. Pyogene Therefore, the prepared Ag-Fe_3O_4/g-C_3N_4 nanocomposite is an excellent candidate for the mitigation of environmental pollutants.

5.2. Recommendation

For future study, this study recommended a few recommendations on the characterization of Ag Fe_3O_4/g-C_3N_4 nanocomposites that will give full information. The elemental distribution and chemical composition of the synthesized samples should be characterized by energy depressive X-ray (EDX) and X-ray photoelectron spectroscopy. In order to investigate the particle size, more detailed morphology, and surface area of nanocomposite should be characterized by TEM and Brunauer–Emmett–Teller (BET) instruments respectively.

Research Fund Acknowledgment

This work is financially supported by Adama Science and Technology University and the Ministry of Innovation and Technology of Ethiopia under the grant number **ASTU/SMR/376/21**, Adama, Ethiopia.

6. Reference

Ahmad, A., Mohd-setapar, S. H., Chuong, S., & Khatoon, A. (2015). RSC Advances Recent advances in new generation dye removal technologies. *Novel search for approaches to reprocess wastewater*,10(3), 308–308. https://doi.org/10.1039/c4ra16959j

Ahmadi, S., Asim, N., Alghoul, M. A., Hammadi, F. Y., Saeedfar, K., Ludin, N. A., Zaidi, S. H., & Sopian, K. (2014). The role of physical techniques on the preparation of photoanodes for dye sensitized solar cells. *International Journal of Photoenergy*, 10, 102–114. https://doi.org/10.1155/2014/198734

Ajayi, E., & Afolayan, A. (2017). Green synthesis, characterization and biological activities of silver nanoparticles from alkalinized Cymbopogon citratus Stapf. *Advances in Natural Sciences, Nanoscience and Nanotechnology*, *8*(1),1–8. https://doi.org/10.1088/2043-6254/aa5cf7

Akhundi, A., & Habibi-Yangjeh, A. (2016). Ternary magnetic g-C_3N_4/Fe_3O_4/AgI nanocomposites: Novel recyclable photocatalysts with enhanced activity in degradation of different pollutants under visible light, *Materials Chemistry and Physics*, *174*, 59–69. https://doi.org/10.1016/j.matchemphys.2016.02.052

Alabdallah, N. M., & Hasan, M. M. (2021). Plant-based green synthesis of silver nanoparticles and its effective role in abiotic stress tolerance in crop plants. *Saudi Journal of Biological Sciences*, *28*(10), 5631–5639. https://doi.org/10.1016/j.sjbs.2021.05.081

Allafchian, A., & Hosseini, S. S. (2019). Antibacterial magnetic nanoparticles for therapeutics: A review. *IET Nanobiotechnology*, *13*(8), 786–799. https://doi.org/10.1049/iet-nbt.2019.0146

Aly, H. F., & Abd-elhamid, A. I. (2018). Photocatalytic Degradation of Methylene Blue Dye Using Silica Oxide Nanoparticles as a Catalyst. *Water environment research. 10, 807–818.* https://doi.org/10.2175/106143017X15131012187953

Amarjargal, A., Tijing, L. D., Im, I. T., & Kim, C. S. (2013). Simultaneous preparation of Ag/Fe_3O_4 core-shell nanocomposites with enhanced magnetic moment and strong antibacterial and catalytic properties. *Chemical Engineering Journal*, *226*, 243–254. https://doi.org/10.1016/j.cej.2013.04.054

Azizi, A. (2020). Green Synthesis of - Fe_3O_4 Nanoparticles and Its Application in Preparation of - Fe 3 O 4 / Cellulose Magnetic Nanocomposite : A Suitable Proposal for Drug Delivery Systems. *Inorganic and Organometallic Polymers and Materials*,10,13-29. https://doi.org/10.1007/s10904-020-01500-1

Baganizi, D. R., Nyairo, E., Duncan, S. A., Singh, S. R., & Dennis, V. A. (2017). Interleukin-10 Conjugation to Carboxylated PVP-Coated Silver Nanoparticles for Improved Stability and Therapeutic Efficacy. *Nanomaterial*, 207, 901-909 https://doi.org/10.3390/nano7070165

Bahrulolum, H., Nooraei, S., & Javanshir, N. (2021). Green synthesis of metal nanoparticles using microorganisms and their application in the agrifood sector. *Journal of Nanobiotechnology*, 20, 1–26. https://doi.org/10.1186/s12951-021-00834-3

Basera, P., Lavania, M., Agnihotri, A., & Lal, B. (2019). Analytical Investigation of Cymbopogon citratus and Exploiting the Potential of Developed Silver Nanoparticle Against the Dominating Species of Pathogenic Bacteria. *Front. Microbio,*.(10),1–13. https://doi.org/10.3389/fmicb.2019.00282

Baudot, C., Tan, C. M., & Kong, J. C. (2010). FTIR spectroscopy as a tool for nano-material characterization. *Infrared Physics and Technology*, *53*(6), 434–438. https://doi.org/10.1016/j.infrared.2010.09.002

Begum, R., Farooqi, Z. H., Naseem, K., Ali, F., Batool, M., Xiao, J., & Irfan, A. (2018). Applications of UV/Vis Spectroscopy in Characterization and Catalytic Activity of Noble Metal Nanoparticles Fabricated in Responsive Polymer Microgels. A Review. *Critical Reviews in Analytical Chemistry*, *48*(6), 503–516. https://doi.org/10.1080/10408347.2018.1451299

Begum, R., Najeeb, J., Sattar, A., Naseem, K., & Irfan, A. (2019). Chemical reduction of methylene blue in the presence of nanocatalysts . *A critical review*, *18*(4), 503–516.https://doi.org/10.1080/10408347.2018.1451299

Campos, E. A., Pinto, D. V. B. S., de Oliveira, J. I. S., Mattos, E. da C., & Dutra, R. de C. L. (2015). Synthesis, characterization and applications of iron oxide nanoparticles - A short review. *Journal of Aerospace Technology and Management*, *7*(3), 267–276.

https://doi.org/10.5028/jatm.v7i3.471

Chahal, C., Akker, B. Van Den, Young, F., & Franco, C. (2016). Pathogen and Particle Associations in Wastewater : Signi fi cance and Implications for Treatment and Disinfection Processes. *In Advances in Applied Microbiology* 97, 503–516. https://doi.org/10.1016/bs.aambs.2016.08.001

Chaki, S. H., Malek, T. J., Chaudhary, M. D., Tailor, J. P., & Deshpande, M. P. (2015). Magnetite Fe_3O_4 nanoparticles synthesis by wet chemical reduction and their characterization. *Advances in Natural Sciences: Nanoscience and Nanotechnology*, *6*(3), 103–116. https://doi.org/10.1088/2043-6262/6/3/035009

Cherian, T., Ali, K., Saquib, Q., Faisal, M., Wahab, R., & Musarrat, J. (2020). Cymbopogon citratus functionalized green synthesis of cuo-nanoparticles: Novel prospects as antibacterial and antibiofilm agents. *Biomolecules*, *10*(2). 13–16. 116.https://doi.org/10.3390/biom10020169

Chirayil, C. J., Abraham, J., Mishra, R. K., George, S. C., & Thomas, S. (2017). Instrumental Techniques for the Characterization of Nanoparticles. *In Thermal and Rheological Measurement Techniques for Nanomaterials Characterization*, *98*, 3–16. https://doi.org/10.1016/B978-0-323-46139-9.00001-3

Dakal, T. C., Kumar, A., Majumdar, R. S., & Yadav, V. (2016). Mechanistic basis of antimicrobial actions of silver nanoparticles. *Frontiers in Microbiology*, 7, 1–17. https://doi.org/10.3389/fmicb.2016.01831

Durán, N., Durán, M., de Jesus, M. B., Seabra, A. B., Fávaro, W. J., & Nakazato, G. (2016), Silver nanoparticles: A new view on mechanistic aspects on antimicrobial activity. *Nanomedicine: Nanotechnology, Biology, and Medicine*, 12(3), 789–799. https://doi.org/10.1016/j.nano.2015.11.016

Dutta, A. (2017), Fourier Transform Infrared Spectroscopy. In *Spectroscopic Methods for Nanomaterials Characterization*, 11(3), 79–85. https://doi.org/10.1016/B978-0-323-46140-5.00004-2

Fakhrul, M., Samsudin, R., & Bacho, N. (2003), Recent Development of Graphitic Carbon Nitride-Based Photocatalyst for Environmental Pollution Remediation. *Nanocatalysts.*

19(3),1–15. http://dx.doi.org/10.5772/intechopen.81639

Franci, G., Falanga, A., Galdiero, S., Palomba, L., Rai, M., Morelli, G., & Galdiero, M. (2015). Silver nanoparticles as potential antibacterial agents. *Molecules*, *20*(5), 8856–8874. https://doi.org/10.3390/molecules20058856

Gamboa, S. M., Rodríguez, E., Martínez, V. V., & Vega-, J. (2019). Synthesis and characterization of silver nanoparticles and their application as an antibacterial agent. *International Journal of Biosensors & Bioelectronics Research*.*5*(5), 56–74. https://doi.org/10.15406/ijbsbe.2019.05.00172

Gan, Y. X., Jayatissa, A. H., Yu, Z., Chen, X., & Li, M. (2020).Hydrothermal Synthesis of Nanomaterials. *Journal of Nanomaterials*, *10*(5), 86–94. https://doi.org/10.1155/2020/8917013

Ganapathe, L. S., Mohamed, M. A., Yunus, R. M., & Berhanuddin, D. D. (2020). Magnetite (Fe_3O_4) nanoparticles in biomedical application: From synthesis to surface functionalisation. *Magnetochemistry*, *6*(4), 1–35. https://doi.org/10.3390/magnetochemistry6040068

Gangadhar, A., Mavinakere, A., & Krishnegowda, J. (2021). Photo-catalytic dye degradation of methylene blue by using ZrO 2 / MWCNT nanocomposites. *nanocatalyst*,16(4), 1265–1276. https://doi.org/10.2166/wpt.2021.066

Gharibshahi, L., Saion, E., Gharibshahi, E., Shaari, A. H., & Matori, K. A. (2017). Structural and Optical Properties of Ag Nanoparticles Synthesized by Thermal Treatment Method. *Material*, 98,1–13. https://doi.org/10.3390/ma10040402

Gudkov, S. V., Burmistrov, D. E., Serov, D. A., Rebezov, M. B., Semenova, A. A., & Lisitsyn, A. B. (2021). Do iron oxide nanoparticles have significant antibacterial properties. *Antibiotics*, *10*(7), 1–23. https://doi.org/10.3390/antibiotics10070884

Guerra, F. D., Attia, M. F., Whitehead, D. C., & Alexis, F. (2018).Nanotechnology for environmental remediation: Materials and applications. *Molecules*, *23*(7), 1–23. https://doi.org/10.3390/molecules23071760

Gupta, A. K., & Ganjewala, D. (2015). Synthesis of Silver Nanoparticles from Cymbopogon flexuosus Leaves Extract and Their Antibacterial Properties. *Australian Journal of Basic*

and Applied Sciences, 8(3), 225–230. https://doi.org/10.1007/s10529-020-03047-0

Hasan, S. (2015). A Review on Nanoparticles : Their Synthesis and Types Biosynthesis : Mechanism. *Research Journal of Recent Sciences*, *4*, 9–11. https://doi.org/10.2174/1573407214666180614121140

Herrmann, J. (2005). Heterogeneous photocatalysis : state of the art and present applications. *Topics in Catalysis*, *3,1-14*. https://doi.org/10.1007/s11244-005-3788-2

Hiremath, L., Narendra Kumar, S., & Sukanya, P. (2018). Development of Antimicrobial Smart Textiles Fabricated with Magnetite Nano Particles Obtained Through Green Synthesis. *Materials Today: Proceedings*, *5*(10), 21030–21039. https://doi.org/10.1016/j.matpr.2018.06.496

Huang, C., Lin, Y., Wang, I., & Lu, C. (2012). Photocatalytic Activity and Characterization of Carbon-Modified Titania for Visible-Light-Active Photodegradation of Nitrogen Oxides. *Research Article*, 99, *1-13*,https://doi.org/10.1155/2012/548647

Huang, J., Ho, W., & Wang, X. (2014). Metal-free disinfection effects induced by graphitic carbon nitride polymers under visible light illumination. *Chemical Communications*, *50*(33), 4338–4340. https://doi.org/10.1039/c3cc48374f

Ijaz, I., Gilani, E., Nazir, A., & Bukhari, A. (2020). Detail review on chemical, physical and green synthesis, classification, characterizations and applications of nanoparticles. *Green Chemistry Letters and Reviews*, *13*(3), 59–81. https://doi.org/10.1080/17518253.2020.1802517

Jabbar, A. H., Al-Janabi, H. S. O., Hamzah, M. Q., Mezan, S. O., Tumah, A. N., Ameruddin, A. S. B., & Agam, M. A. (2020). Green synthesis and characterization of silver nanoparticle (Ag NPs) using pandanus atrocarpus extract. *International Journal of Advanced Science and Technology*, *29*(3), 4913–4922. https://doi.org/10.1021/jacs.5b11411

Jacinto, M. J., Silva, V. C., Valladão, D. M. S., & Souto, R. S. (2021). Biosynthesis of magnetic iron oxide nanoparticles: a review. *Biotechnology Letters*, *43*(1), 1–12. https://doi.org/10.1007/s10529-020-03047-0

Jana, T. K., Maji, S. K., Pal, A., Maiti, R. P., Dolai, T. K., & Chatterjee, K. (2016).

Photocatalytic and Antibacterial Activity of Cadmium Sulphide / Zinc Oxide Nanocomposite with Varied Morphology. *Journal of Colloid And Interface Science*.12 (9),73 -79, https://doi.org/10.1016/j.jcis.2016.06.073

Joo, H., Chan, K., Park, H., & Sang, C. (2015). One pot synthesis and characterization of Ag-ZnO/g-C_3N_4 photocatalyst with improved photoactivity and antibacterial properties. *Colloids and Surfaces A: Physicochem. Eng. Aspects*, https://doi.org/10.1016/j.colsurfa.2015.07.003

Kaur, S., & Kaur, P. (2019). Nanoparticles Characterization and Applications: An Overview. *Indo Global Journal of Pharmaceutical Sciences*, *09*(02), 146–146. https://doi.org/10.35652/igjps.2019.92s44

Khaghani, S., & Ghanbari, D. (2016). Magnetic and photo-catalyst Fe_3O_4 – Ag nanocomposite : green preparation of silver and magnetite nanoparticles by garlic extract. *Journal of Materials Science: Materials in Electronics*, 70, 4–6. https://doi.org/10.1007/s10854-016-5872-8

Khan, Z. U. H., Khan, A., Shah, A., Wan, P., Chen, Y., Khan, G. M., Khan, A. U., Tahir, K., Muhammad, N., & Khan, H. U. (2016). Enhanced photocatalytic and electrocatalytic applications of green synthesized silver nanoparticles. *Journal of Molecular Liquids*, *220*, 248–257. https://doi.org/10.1016/j.molliq.2016.04.082

Kong, X., Liu, X., Zheng, Y., Chu, P. K., Zhang, Y., & Wu, S. (2021). Graphitic carbon nitride-based materials for photocatalytic antibacterial application. *Materials Science and Engineering R: Reports*, *145*(5), 48–57. https://doi.org/10.1016/j.mser.2021.100610

Kumar, A., & Kumar, P. (2016). Nickel Decorated on Phosphorous-Doped Carbon Nitride as an Efficient Photocatalyst for Reduction of Nitrobenzenes Nickel Decorated on Phosphorous-Doped Carbon Nitride as an Efficient Photocatalyst for Reduction of Nitrobenzenes. *Nanomaterial.* 104, 28–36. https://doi.org/10.3390/nano6040059

Promila, P. (2020). A Review on the Phytochemistry and Pharmacology of Cymbopogon citratus A Review on the Phytochemistry and Pharmacology of Cymbopogon citratus Stapf . *thepharmajournal*,9 (12), 1-8. http://dx.doi.org/10.1155/2015/682749

Li, Xin, Yu, J., & Jiang, C. (2020). Principle and surface science of photocatalysis. *In*

Interface Science and Technology, 31, 1-38. https://doi.org/10.1016/B978-0-08-102890-2.00001-4

Li, Xuanxuan, Spence, J. C. H., Hogue, B. G., & Liu, H. (2017). Merging single-shot XFEL diffraction data from inorganic nanoparticles: *A new approach to size and orientation determination. IUCrJ*, *4*, 741–750. https://doi.org/10.1107/S2052252517012398

Ling, Y., Lim, S., Chyuan, H., & Tong, W. (2016). Research progress on iron oxide-based magnetic materials : Synthesis techniques and photocatalytic applications. *Ceramics International*, *42*(1), 9–34. https://doi.org/10.1016/j.ceramint.2015.08.144

Liu, R., Yang, W., He, G., Zheng, W., Li, M., Tao, W., & Tian, M. (2020). *Ag-Modi fied g -C_3 N_4 Prepared by a One-Step Calcination Method for Enhanced Catalytic E ffi ciency and Stability*, *29*(3), 119–130. https://doi.org/10.1021/acsomega.0c02161

Marimuthu, S., Jayanthi, A., & Malayandi, S. (2020). A review on synthesis , treatment methods , mechanisms , photocatalytic degradation , toxic effects and mitigation of toxicity. *Journal of Photochemistry & Photobiology, B: Biology*, *205*, 111-123. https://doi.org/10.1016/j.jphotobiol.2020.111823

Mathur, P., Jha, S., Ramteke, S., & Jain, N. K. (2018). Pharmaceutical aspects of silver nanoparticles. *Artificial Cells, Nanomedicine and Biotechnology*, *46*(1), 115–126. https://doi.org/10.1080/21691401.2017.1414825

Mavaei, M., Chahardoli, A., Shokoohinia, Y., & Khoshroo, A. (2020). One-step Synthesized Silver Nanoparticles Using Isoimperatorin : Evaluation of Photocatalytic , and Electrochemical Activities. *Scintific research.* 107, 1–12. https://doi.org/10.1038/s41598-020-58697-x

Mekdes. (2021). Remediation of textile industry organic dye waste by photocatalysis using eggshell impregnated ZnO/CuO nanocomposite 65, 2753–2761. https://doi.org/10.2166/wst.2021.165

Meskelu, E. (2019). Irrigation & Drainage Systems Engineering Response of Lemongrass (Cympopogon citratus (DC) Stapf) to Deficit Irrigation and Furrow Irrigation Water Application Methods at Wondo. *Irrigation & Drainage Systems Engineering*, 8,1-6. https://doi.org/10.4172/2168-9768.1000230

Mirabello, G., Lenders, J. J. M., & Sommerdijk, N. A. J. M. (2016). Chem Soc Rev Bioinspired synthesis of magnetite nanoparticles, 45, 12–14. *This journal is©The Royal Society of Chemistry*. https://doi.org/10.1039/c6cs00432f

Mishra, P., Patnaik, S., & Parida, K. (2019). An overview of recent progress on noble metal modified magnetic Fe_3O_4 for photocatalytic pollutant degradation and H_2 evolution. *Catalysis Science and Technology*, *9*(4), 916–941. https://doi.org/10.1039/c8cy02462f

Mohamad, N. A. N., Arham, N. A., & Junaidah, J. (2014). Green synthesis of magnetite (Fe_3O_4) nanoparticles using Graptophyllum pictum leaf aqueous extract Green synthesis of magnetite (Fe_3O_4) nanoparticles using Graptophyllum pictum leaf aqueous extract. *Materials Science and Engineering*. *11*(3), 916–941PAPER https://doi.org/10.1088/1757-899X/191/1/012014

Mohamed, R. M., Mkhalid, I. A., Baeissa, E. S., & Al-Rayyani, M. A. (2012). Photocatalytic degradation of methylene blue by Fe/ZnO/SiO_2 nanoparticles under visiblelight. *Journal of Nanotechnology*, *201, 112-117*. https://doi.org/10.1155/2012/329082

Mohammadlou, M., Maghsoudi, H., & Jafarizadeh-Malmiri, H. (2016). A review on green silver nanoparticles based on plants: Synthesis, potential applications and eco-friendly approach. *International Food Research Journal*, *23*(2), 446–463. Journal homepage: http://www.ifrj.upm.edu.

Mohanraj, J., Durgalakshmi, D., & Saravanan, R. (2020). *Jo ur na l P re of. Environmental Pollution*, *13*(2), 46–63. https://doi.org/10.1016/j.envpol.2020.116172

Mohapatra, M., & Anand, S. (2010). *Synthesis and applications of nano-structured iron oxides / hydroxides – a review*. *2*(8), 127–146. https://doi.org/10.5620/eaht.20210012

Mourdikoudis, S., Pallares, R. M., & Thanh, N. T. K. (2018). Characterization techniques for nanoparticles: Comparison and complementarity upon studying nanoparticle properties. *Nanoscale*, *10*(27), 12871–12934. https://doi.org/10.1039/c8nr02278j

Mulushewa, Z., Dinbore, W. T., & Ayele, Y. (2021). Removal of methylene blue from textile waste water using kaolin and zeolite-x synthesized from Ethiopian kaolin. *Environmental Analysis Health and Toxicology*, *36*(1), 202-207. https://doi.org/10.5620/eaht.2021007

Nakamura, S., Sato, M., Sato, Y., Ando, N., Takayama, T., Fujita, M., & Ishihara, M. (2019).

Synthesis and application of silver nanoparticles (Ag nps) for the prevention of infection in healthcare workers. *International Journal of Molecular Sciences*, *20*(15), 1-18. https://doi.org/10.3390/ijms20153620

Natarajan, S., Harini, K., Gajula, G. P., Sarmento, B., Teresa, M., Petersen, N., & Thiagarajan, V. (2019). Multifunctional magnetic iron oxide nanoparticles : diverse synthetic approaches , surface modifications , cytotoxicity towards biomedical and industrial applications. *BMC Materials*,107, 1–22. https://doi.org/10.1186/s42833-019-0002-6

Natsuki, J., Natsuki, T., & Hashimoto, Y. (2015). A Review of Silver Nanoparticles : Synthesis Methods , Properties and Applications. *4*(5), 325–332. *International Journal of Materials Science and Applications*.https://doi.org/10.11648/j.ijmsa.20150405.17

Nguyen Thi Thu, T., Nguyen Thi, N., Tran Quang, V., Nguyen Hong, K., Nguyen Minh, T., & Le Thi Hoai, N. (2016). Synthesis, characterisation, and effect of pH on degradation of dyes of copper-doped TiO2. *Journal of Experimental Nanoscience*, *11*(3), 226–238. https://doi.org/10.1080/17458080.2015.1053541

Nguyen, V. H., & Mousavi, M. (2020). Synthesis, characterization, and photocatalytic performance of $Ag/AgFeO_2$ decorated on g-C_3N_4-nanosheet under the visible light irradiation. *Journal of the Taiwan Institute of Chemical Engineers*, *115*, 279–292. https://doi.org/10.1016/j.jtice.2020.10.009

Nnadozie, E. C., & Ajibade, P. A. (2020). Green synthesis and characterization of magnetite (Fe3O4) nanoparticles using Chromolaena odorata root extract for smart nanocomposite. *Materials Letters*, *263*, 127-145. https://doi.org/10.1016/j.matlet.2019.127145

Ojha, A. (2020). Nanomaterials for removal of waterborne pathogens : opportunities and challenges. In *Waterborne Pathogens: Detection and Treatment*. Elsevier. *13 (12)*, 107-115. https://doi.org/10.1016/B978-0-12-818783-8.00019-0

Padmavathy, S., & Elangovan, A. (2017). US CR. Journal of Photochemistry & Photobiology. *B: Biology. 103*, 10-25 https://doi.org/10.1016/j.jphotobiol.2017.03.018

Pant, B., Park, M., & Hee, J. (2017). Journal of Colloid and Interface Science Novel magnetically separable silver-iron oxide nanoparticles decorated graphitic carbon nitride nano-sheets : A multifunctional photocatalyst via one-step hydrothermal process. *Journal*

of Colloid And Interface Science, *496*, 343–352. https://doi.org/10.1016/j.jcis.2017.02.012

Pant, B., Park, M., Lee, J. H., Kim, H. Y., & Park, S. J. (2017). Novel magnetically separable silver-iron oxide nanoparticles decorated graphitic carbon nitride nano-sheets: A multifunctional photocatalyst via one-step hydrothermal process. In *Journal of Colloid and Interface Science*, 496, 1-31. https://doi.org/10.1016/j.jcis.2017.02.012

Patiño-Ruiz, D., Sánchez-Botero, L., Tejeda-Benitez, L., Hinestroza, J., & Herrera, A. (2020). Green synthesis of iron oxide nanoparticles using Cymbopogon citratus extract and sodium carbonate salt: Nanotoxicological considerations for potential environmental applications. *Environmental Nanotechnology, Monitoring and Management*, *14*, 1-9. https://doi.org/10.1016/j.enmm.2020.100377

Pattabi, R. M., & Pattabi, M. (2013). Antibacterial applications of silver nanoparticles. *Materials Science Forum*, *754*, 131–142. https://doi.org/10.4028/www.scientific.net/MSF.754.131

Qi, L., Zhang, K., Qin, W., & Hu, Y. (2020). Highly e ffi cient fl ow-through catalytic reduction of methylene blue using silver nanoparticles functionalized cotton. *Chemical Engineering Journal*, *388*, 124-132. https://doi.org/10.1016/j.cej.2020.124252

Radhakrishnan, E. K. (2018). Rapid Degradative Effect of Microbially Synthesized Silver Nanoparticles on Textile Dye in Presence of Sunlight. *Biocatalysis and Agricultural*, 17, 1-12. https://doi.org/10.1016/j.bcab.2018.04.007

Roy, A., Bulut, O., Some, S., Mandal, A. K., & Yilmaz, M. D. (2019). Green synthesis of silver nanoparticles: Biomolecule-nanoparticle organizations targeting antimicrobial activity. In *RSC Advances*, 9, (5),1-9. https://doi.org/10.1039/c8ra08982e

Ruíz-baltazar, Á. D. J., & Reyes-lópez, S. Y. (2019). Results in Physics Eco-friendly synthesis of Fe_3O_4 nanoparticles : Evaluation of their catalytic activity in methylene blue degradation by kinetic adsorption models. *Results in Physics*, *12*, 989–995. https://doi.org/10.1016/j.rinp.2018.12.037

Saeed, M., Usman, M., & Haq, A. ul. (2018). Catalytic Degradation of Organic Dyes in Aqueous Medium. *Photochemistry and Photophysics - Fundamentals to Applications*, 12,

109-117. https://doi.org/10.5772/intechopen.75008

Sahoo, C., Gupta, A. K., & Sasidharan Pillai, I. M. (2012). Photocatalytic degradation of methylene blue dye from aqueous solution using silver ion-doped TiO_2 and its application to the degradation of real textile wastewater. *Journal of Environmental Science and Health - Part A Toxic/Hazardous Substances and Environmental Engineering*, *47*(10), 1428–1438. https://doi.org/10.1080/10934529.2012.672387

Said, R. A. M., Hasan, M. A., Abdelzaher, A. M., & Abdel-raoof, A. M. (2020). Review — Insights into the Developments of Nanocomposites for Its Processing and Application as Sensing Materials Review — Insights into the Developments of Nanocomposites for Its Processing and Application as Sensing Materials. *Journal of the Electrochemical Society, 167, 1-9.* https://doi.org/10.1149/1945-7111/ab697b

Sajid, M., & Płotka-Wasylka, J. (2020). Nanoparticles: Synthesis, characteristics, and applications in analytical and other sciences. *Microchemical Journal*, *154*, 104-123. https://doi.org/10.1016/j.microc.2020.104623

Sajjadi, M., Nasrollahzadeh, M., & Mohammad Sajadi, S. (2017). Green synthesis of Ag/Fe3O4 nanocomposite using Euphorbia peplus Linn leaf extract and evaluation of its catalytic activity. *Journal of Colloid and Interface Science*, *497*, 1–13. https://doi.org/10.1016/j.jcis.2017.02.037

Sandhya, M., & Ramandeep, K. (2017). *Asian Journal of*. *6*(8), 58–70. https://doi.org/10.1088/1757-899X/191/1/01207

Sari, I. P., & Yulizar, Y. (2017). Green synthesis of magnetite (Fe_3O_4) nanoparticles using Graptophyllum pictum leaf aqueous extract. *IOP Conference Series: Materials Science and Engineering*, *191*(1). https://doi.org/10.1088/1757-899X/191/1/012014

Shabina, S., Gaurav, S., Irfan, A. M., & Sarmad, M. (2020). Green nanotechnology: A review on nanomedicinal potential and green synthesis of silver nanoparticles (ag-np's). *Research Journal of Biotechnology*, *15*(10), 177–187. https://doi.org/10.1088/1757-899X/191/1/012020

Sharma, D., Kanchi, S., & Bisetty, K. (2019). Biogenic synthesis of nanoparticles : A review. *Arabian Journal of Chemistry*, *12*(8), 3576–3600.

https://doi.org/10.1016/j.arabjc.2015.11.002

Singh, J., Kumar, V., Singh, S., Kim, K., Rawat, M., Kukkar, D., & Fai, Y. (2019). Journal of Industrial and Engineering Chemistry Biogenic synthesis of silver nanoparticles and its photocatalytic applications for removal of organic pollutants in water. *Journal of Industrial and Engineering Chemistry*, *80*, 247–257. https://doi.org/10.1016/j.jiec.2019.08.002

Singh, V., Yadav, P., & Mishra, V. (2020). Recent Advances on Classification, Properties, Synthesis, and Characterization of Nanomaterials. *Green Synthesis of Nanomaterials for Bioenergy Applications*, 9, 83–97. https://doi.org/10.1002/9781119576785.ch3

Syafiuddin, A., Salmiati, Salim, M. R., Beng Hong Kueh, A., Hadibarata, T., & Nur, H. (2017). A Review of Silver Nanoparticles: Research Trends, Global Consumption, Synthesis, Properties, and Future Challenges. *Journal of the Chinese Chemical Society*, *64*(7), 732–756. https://doi.org/10.1002/jccs.201700067

Tarannum, N., & Gautam, Y. K. (2019). Facile green synthesis and applications of silver nanoparticles: a state-of-the-art review. nanoparticle*s : A state-of-the-art review*, 12, 34926–34948. https://doi.org/10.1039/c9ra04164h

Thamilselvi, V., & Radha, K. V. (2018). A Review On The Diverse Application Of Silver Nanoparticle. *IOSR Journal Of Pharmacy*, 7 (1), 21-27 https://doi.org/10.9790/3013-0701012127

Thurston, J. H., Hunter, N. M., Wayment, L. J., & Cornell, K. A. (2017). Urea-derived graphitic carbon nitride (u-g-C_3N_4) films with highly enhanced antimicrobial and sporicidal activity. *Journal of Colloid and Interface Science*, *505*, 910–918. https://doi.org/10.1016/j.jcis.2017.06.089

Tju, H., Shabrany, H., Taufik, A., & Saleh, R. (2017). Degradation of methylene blue (MB) using ZnO/CeO2/nanographene platelets (NGP) photocatalyst: Effect of various concentration of NGP. *AIP Conference Proceedings*, *1862*(2017). https://doi.org/10.1063/1.4991141

Torres, T. E., Ibarra, M. R., & Goya, G. F. (2009). Fe_3O_4 Nanoparticles for Biomedical Applications . *Colloids and Surfaces B: Biointerfaces*, *6*(1), 2008–2009.

https://doi.org/10.1016/j.colsurfb.2018.02.031

Vanlalveni, C., Lallianrawna, S., Biswas, A., Selvaraj, M., Changmai, B., & Rokhum, S. L. (2021). Green synthesis of silver nanoparticles using plant extracts and their antimicrobial activities: a review of recent literature. *RSC Advances*, *11*(5), 2804–2837. https://doi.org/10.1039/d0ra09941d

Venkateswarlu, S., Natesh Kumar, B., Prathima, B., Anitha, K., & Jyothi, N. V. V. (2015). A novel green synthesis of Fe_3O_4-Ag core shell recyclable nanoparticles using Vitis vinifera stem extract and its enhanced antibacterial performance. *Physica B: Condensed Matter*, *457*, 30–35. https://doi.org/10.1016/j.physb.2014.09.007

Viju Kumar, V. G., & Prem, A. A. (2018). Green synthesis and characterization of iron oxide nanoparticles using phyllanthus niruri extract. *Oriental Journal of Chemistry*, *34*(5), 2583–2589. https://doi.org/10.13005/ojc/340547

Wang, K. (2019). Degradation of methylene blue with magnetic Co- doped Fe_3O_4 @ FeOOH nanocomposites as heterogeneous catalysts of peroxymonosulfate, 12, 17664–17673. https://doi.org/10.1039/c9ra01671f

Wang, Y., Pan, F., Dong, W., Xu, L., Wu, K., & Xu, G. (2016). Applied Catalysis B : Environmental Recyclable silver-decorated magnetic titania nanocomposite with enhanced visible-light photocatalytic activity. *"Applied Catalysis B, Environmental," 189*, 192–198. https://doi.org/10.1016/j.apcatb.2016.02.057

Xiao,Y., Donga, Z., & Wei, G. (2015). Nanosilver As A New Generation of Silver Catalysts in Organic Transformations for Efficient Synthesis of Fine Chemicals. *Catalysis Science & Technology*,121, 1-19. https://doi.org/10.1039/C5CY00285K

Xin, Q., Shah, H., Nawaz, A., Xie, W., Akram, M. Z., Batool, A., Tian, L., Jan, S. U., Boddula, R., Guo, B., Liu, Q., & Gong, J. R. (2019). Antibacterial Carbon-Based Nanomaterials. *Advanced Materials*, *31*(45), 1–15. https://doi.org/10.1002/adma.201804838

Yang, J., Chen, H., Gao, J., Yan, T., Zhou, F., Cui, S., & Bi, W. (2016). Synthesis of Fe_3O_4/g-C_3N_4 nanocomposites and their application in the photodegradation of 2,4,6-trichlorophenol under visible light. *Materials Letters*, *164*, 183–189.

https://doi.org/10.1016/j.matlet.2015.10.130

Yasin, S. A., Yaseen, S., Zeebaree, S., Yaseen, A., & Zeebaree, S. (2021). *The Efficient Removal of Methylene Blue Dye Using CuO / PET Nanocomposite in Aqueous Solutions*, 9, 1–14. https://doi.org/10.1002/adma.201804823456

Yew, Y. P., Shameli, K., Miyake, M., Kuwano, N., Bt Ahmad Khairudin, N. B., Bt Mohamad, S. E., & Lee, K. X. (2016). Green Synthesis of Magnetite (Fe_3O_4) Nanoparticles Using Seaweed (Kappaphycus alvarezii) Extract. *Nanoscale Research Letters*, *11*(1). 11-17. https://doi.org/10.1186/s11671-016-1498-2

Yin, I. X., Zhang, J., Zhao, I. S., Mei, M. L., Li, Q., & Chu, C. H. (2020). The antibacterial mechanism of silver nanoparticles and its application in dentistry. *International Journal of Nanomedicine*, *15*, 2555–2562. https://doi.org/10.2147/IJN.S246764

Yusuf, M. (2019). Silver Nanoparticles: Synthesis and Applications. *Springer Nature Switzerland. 12,* 2343–2356. https://doi.org/10.1007/978-3-319-68255-6_16

Zhang, G. and D. (2020). Graphitic carbon nitride-based materials for photocatalytic reduction of U(VI)*rsc.li/njc*,11, 1-35. https://doi.org/10.1039/D0NJ04519E

Zhang, S., Li, J., Wang, X., Huang, Y., Zeng, M., & Xu, J. (2014). Strongly Coupled Ag@AgClg‑C_3N_4. *ACS Applied Materials & Interfaces,* 22, 115-123. *dx.doi.org/10.1021/am505528c*

Zhao, Z., Fan, J., Xue, Y., Chang, H., Masubuchi, Y., & Yin, S. (2017). SC. *Journal of Alloys and Compounds,* 10, 104-1012. https://doi.org/10.1016/j.jallcom.2017.11.033

Zheng, Y., Zhang, Z., & Li, C. (2016). A comparison of graphitic carbon nitrides synthesized from different precursors through pyrolysis. *Journal of Photochemistry & Photobiology, A: Chemistry, 19, 1-32.* https://doi.org/10.1016/j.jphotochem.2016.08.005

Zou, X., Zhang, L., Wang, Z., & Luo, Y. (2016). Mechanisms of the Antimicrobial Activities of Graphene Materials. *Journal of the American Chemical Society*, *138*(7), 2064–2077. https://doi.org/10.1021/jacs.5b11411